Electronic Supplementary Information (ESI)

Molecular design of thermally activated delayed fluorescence properties of phenazine-5,10-diyl-dibenzonitriles†

Dietrich Püschel,[1] Julia Wiefermann,[2] Simon Hédé,[3] Tobias Heinen,[1] Leo Pfeifer,[1] Oliver Weingart,[3,*] Markus Suta,[1,*] Thomas J. J. Müller,[2,*] Christoph Janiak[1,*]

1 Institut für Anorganische Chemie und Strukturchemie, Heinrich-Heine-Universität Düsseldorf, Universitätsstraße 1, D-40225 Düsseldorf, Germany
E-Mail: Markus.Suta@hhu.de, Janiak@uni-duesseldorf.de
2 Institut für Organische Chemie und Makromolekulare Chemie, Heinrich-Heine-Universität Düsseldorf, Universitätsstraße 1, D-40225 Düsseldorf, Germany
E-Mail: ThomasJJ.Mueller@hhu.de
3 Institute for Theoretical Chemistry and Computational Chemistry, Heinrich-Heine-Universität Düsseldorf, Universitätsstraße 1, D-40225 Düsseldorf, Germany
E-mail: Oliver.Weingart@hhu.de

Emails: dietrich.pueschel@hhu.de, julia.wiefermann@hhu.de, hede@hhu.de, t.heinen@hhu.de, leo.pfeifer@hhu.de, Oliver.Weingart@hhu.de, markus.suta@hhu.de, thomasJJ.Mueller@hhu.de, janiak@hhu.de

Content

S1 Sources of chemicals

Commercially available reagents were used without further purification.

Items	Manufacturer
Phenazine, 97 %	BLDpharm
3-Bromobenzonitrile	BLDpharm
4-Bromobenzonitrile	fluorochem
4'-Bromo-[1,1'-biphenyl]-4-carbonitrile, 95 %	BLDpharm
Palladium(II) acetate, 98 %	Sigma-Aldrich
Tri-*tert*-butyl-phosphine	Sigma-Aldrich
Sodium dithionite	VWR Chemicals
Sodium chloride, ≥ 99.5 %	Sigma-Aldrich
Magnesium sulfate	VWR Chemicals
Potassium carbonate	Riedel-de Haen
Toluene, ≥ 99.7 %	Sigma-Aldrich
Ethanol, ≥ 99.8 %	Honeywell
Dichloromethane, ≥ 99.9 %	Sigma-Aldrich
Chloroform, ≥ 99.8 %	Fisher Chemical
n-Hexane, ≥ 99.0 %	VWR Chemicals
Cyclohexane, ≥ 99.8 %	Fisher Chemical

S2 Synthesis

S2.1 5,10-Dihydrophenazine

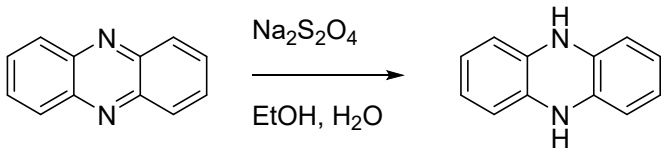

5,10-Dihydrophenazine
Chemical formula $C_{12}H_{10}N_2$
Molecular weight: 182.23

Starting materials	***M* / g·mol⁻¹**	***ρ* / g·cm⁻³**	**eq**	***n* / mmol**	***m* / g**	***V* / mL**
Phenazine	180.21	-	1.0	27.7	5.00	-
Sodium dithionite	174.11	2.38	10.0	277.0	48.2	-

Following literature procedures,[1,2] phenazine was dissolved in ethanol (125 mL), sodium dithionite in de-ionized water (500 mL) and both solutions were combined and heated under stirring and reflux for three hours or overnight. The precipitate was filtered off and washed three times with deionized water. Finally, the solid was dried at 20 °C in vacuum (1x10^{-3} mbar) for 16 h. The product (yield 4.75 g, 94 %) was obtained as a light green solid and was used without further purification. Important: The dihydrophenazine solid must be stored under a protective gas atmosphere (nitrogen or argon), otherwise it re-oxidizes which is evidenced by slowly turning dark blue and then black.

[^{1}**H NMR**] (600 MHz, $CDCl_3$) δ = 8.27 (dd, *J* = 6.8, 3.5 Hz, 1H), 7.86 (dd, *J* = 6.8, 3.4 Hz, 1H), 6.12 (s, 2H), 1.57 (s, 3H).

S2.2 4,4'-(Phenazine-5,10-diyl)dibenzonitrile (pBN)

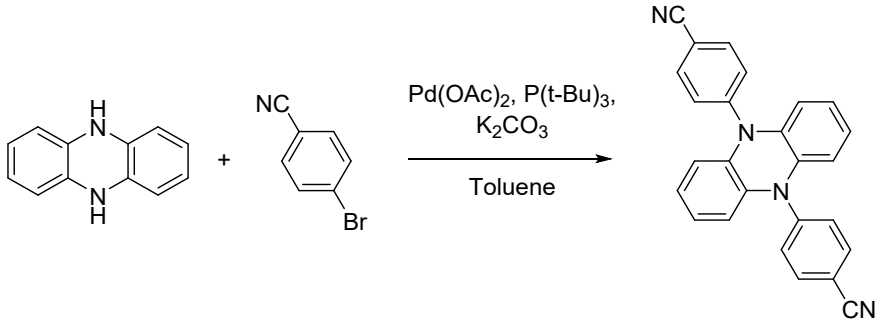

4,4'-(Phenazine-5,10-diyl)dibenzonitrile
Chemical Formula: $C_{26}H_{16}N_4$
Molecular Weight: 384.44

Starting materials	***M* / g·mol⁻¹**	***ρ* / g·cm⁻³**	**eq**	***n* / mmol**	***m* / g**	***V* / mL**
5,10-Dihydrophenazine	182.22	-	1.00	5.49	1.00	-
4-Bromobenzonitrile	182.02	-	2.20	12.1	2.20	-
Potassium carbonate	138.20	2.43	6.00	32.9	4.55	-
Palladium(II) acetate	224.51	-	5 mol%		0.061	-
Tri-*tert*-butyl-phosphine	202.32	0.83	10 mol%		0.111	134

Following literature procedures,[1,2] 5,10-dihydrophenazine, 4-bromobenzonitrile and potassium carbonate were dissolved in degassed toluene (20 mL). Palladium(II) acetate and tri-*tert*-butylphosphine were dissolved in degassed toluene (20 mL). Both solutions were combined under stirring. Under nitrogen inert gas the reaction mixture was heated with stirring to reflux for 24 hours. After cooling to room temperature, water (60 mL) was added to the reaction mixture and the water/toluene mixture extracted three times with chloroform (3 x 200 mL). The organic phases were combined, washed with a brine, dried over magnesium sulfate (5 min) and concentrated using a rotary evaporator. After addition of n-hexane (20 mL), a golden yellow insoluble precipitate was formed. The precipitated raw product was filtered off and washed three times with 60 mL each of a mixture of n-hexane/chloroform (2:1) and dried at 20 °C under vacuum (1x10^{-3} mbar) for 16 h. The product was obtained as a golden yellow crystalline solid (yield 1.6 g, 76 %). Ideally, the product occurs as small yellow-gold crystals. To increase the yield, the crystallisation solution can be concentrated and purified by column chromatography (dichloromethane/cyclohexane 10:1).

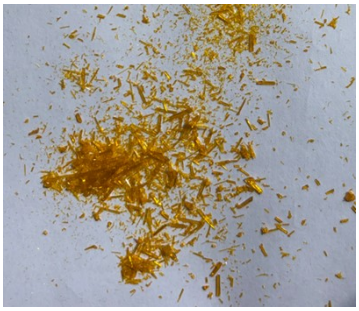

[**^{1}H NMR**] (600 MHz, C_6D_6) δ = 6.96 (d, *J* = 8.2 Hz, 4H), 6.71 (d, *J* = 8.2 Hz, 4H), 6.41 – 6.37 (m, 4H), 5.69 (dt, *J* = 7.9, 3.9 Hz, 4H).
[**HR-ESI-MS**] (m/z): Calc. for [M$^+$]: 384.1375 – found: 384.1370
[**EA**] Calc. for $C_{26}H_{16}N_4$: C 81.20, H 4.20, N 14.57 – found: C 80.7, H 4.21, N 14.39 %
[**M.p**] > 300 °C

S2.3 3,3'-(Phenazine-5,10-diyl)dibenzonitrile (mBN)

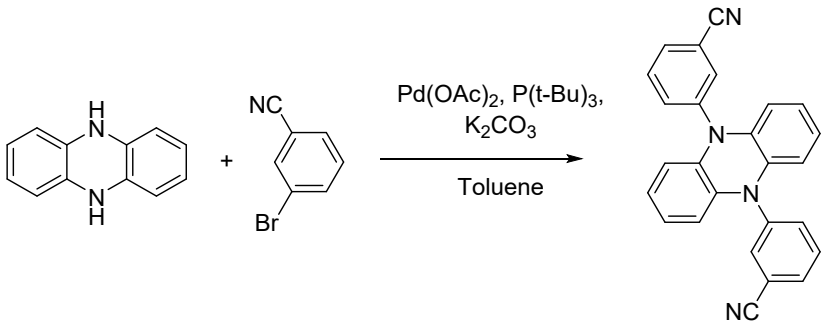

3,3'-(Phenazine-5,10-diyl)dibenzonitrile
Chemical Formula: $C_{26}H_{16}N_4$
Molecular Weight: 384.44

Starting materials	M / g·mol^{-1}	ρ / g·cm^{-3}	eq	n / mmol	m / g	V / mL
5,10-Dihydrophenazine	182.22	-	1.00	5.49	1.00	-
3-Bromobenzonitrile	182.02	-	2.20	12.1	2.20	-
Potassium carbonate	138.20	2.43	6.00	32.9	4.55	-
Palladium(II) acetate	224.51	-	5 mol%		0.061	-
Tri-*tert*-butylphosphine	202.32	0.83	10 mol%		0.111	134

Following the procedure in S2.2 the starting materials 5,10-dihydrophenazine, 3-bromobenzonitrile and potassium carbonate were dissolved in toluene (20 mL). Palladium(II) acetate and tri-*tert*-butylphosphine were dissolved in toluene (20 mL). Both solutions were combined under stirring. Under nitrogen inert gas the reaction mixture was heated with stirring to reflux for 24 hours.[3] After cooling to room temperature, water (60 mL) was added to the reaction mixture and the water/toluene mixture extracted three times with chloroform (3 x 200 mL). The organic phases were combined, washed with a saturated aqueous NaCl solution (~ 25 %), dried over magnesium sulfate (5 min) and concentrated using a rotary evaporator. After 3 d and slow evaporation of the solvent, yellow crystals precipitated. The precipitated raw product was filtered off and washed three times with 60 mL each of a mixture of n-hexane/chloroform (2:1) and dried at 20 °C under vacuum (1x10^{-3} mbar) for 16 h. The product was obtained as small yellow crystals (yield 1.67 g, 79 %).To increase the yield, the crystallization solution can be concentrated and purified by column chromatography (dichloromethane/cyclohexane 10:1).

[^{1}**H NMR**] (300 MHz, C_6D_6) δ = 7.47 (s, 2H), 7.45 – 7.30 (m, 6H), 6.53 - 6.47 (m, 4H), 5.80 - 5.73 (m, 4H)
[**HR-ESI-MS**] (m/z): Calc. for [M$^+$]: 384.1375 – found: 384.1367
[**EA**] Calc. for $C_{26}H_{16}N_4$: C 81.20, H 4.20, N 14.57 – found: C 81.41, H 4.27, N 14.51 %
[**M.p**] 284 °C

S2.4 4',4'''-(Phenazine-5,10-diyl)bis(([1,1'-biphenyl]-4-carbonitrile)) (BPN)

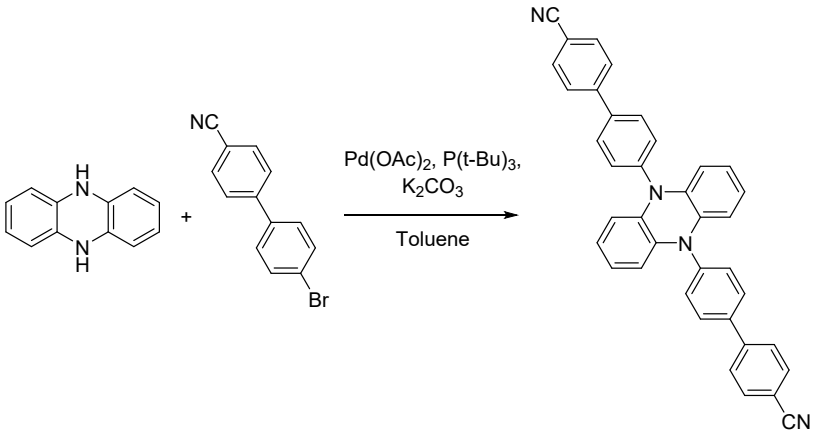

4',4'''-(phenazine-5,10-diyl)bis(([1,1'-biphenyl]-4-carbonitrile))
Chemical Formula: $C_{38}H_{24}N_4$
Molecular Weight: 536,64

Starting materials	***M* / g·mol⁻¹**	***ρ* / g·cm⁻³**	**eq**	***n* / mmol**	***m* / g**	***V* / mL**
5,10-Dihydrophenazine	182.22	-	1.00	5.49	1.00	-
4'-Bromo-[1,1'-biphenyl]-4-carbonitrile	258.12	-	2.20	12.0	3.10	-
Potassium carbonate	138.20	2.43	6.00	32.9	4.55	-
Palladium(II) acetate	224.51	-	8 mol%		0.098	-
Tri-*tert*-butylphosphin	202.32	-	16 mol%		0.178	-

Following the procedure in S2.2 the starting materials 5,10-dihydrophenazine, 4'-bromo-[1,1'-biphenyl]-4-carbonitrile, and potassium carbonate were dissolved in degassed toluene (20 mL). Palladium(II) acetate and tri-*tert*-butylphosphine were dissolved in degassed toluene (20 mL). Both solutions were combined under stirring. Under nitrogen inert gas the reaction mixture was heated with stirring to reflux for 48 hours. The solvent toluene was removed by rotary evaporator. The crude product (dark orange/brown to black) was dissolved and resuspended in hot chloroform and filtered using a short (10 cm) filter column (silica). The filter cake was washed with hot chloroform until the filtrate became colorless (approximately 250 mg of product dissolves in 1 L of hot chloroform). The chloroform filtrates were combined and the solvent concentrated to about 200 mL using a rotary evaporator. The crystallized product was filtered and washed three times with chloroform (20 mL). The product was obtained as fine orange crystals (yield 2.06 g, 70 %).

[^{1}**H NMR**] (600 MHz, C_6D_6) δ = 7.54 – 7.49 (m, 1H), 7.32 – 7.25 (m, 2H), 7.24 – 7.19 (m, 1H), 7.14 – 7.10 (m, 25H), 7.10 – 7.05 (m, 1H), 7.03 – 6.97 (m, 1H).
[**HR-ESI-MS**] (m/z): Calc. for [M^+]: 536.2001 – found: 536.1998
[**EA**] Calc. for $C_{38}H_{24}N_4$: C 85.05, H 4.51, N 10.44 – found: C 85.67, H 4.43, N 10.52 %
[**M.p**] > 300 °C

S3 Crystal structure details

The sample of **β-pBN** crystallized via slow evaporation of a $CHCl_3$ solution as yellow elongated blocks/needles with a nearly rectangular (rather trapeze) cross section. A suitable crystal was mounted on a microloop in a drop of immersion oil. For 4,4'-(phenazine-5,10-diyl)dibenzonitrile (**pBN**, β-polymorph) the data was collected using φ and ω-scans on a Bruker Kappa APEX 2 CCD X-ray diffractometer with a microfocus sealed tube, Mo-Kα radiation (λ = 0.71073 Å), and a multi-layer mirror monochromator. For the compounds 3,3'-(phenazine-5,10-diyl)dibenzonitrile (**mBN**) and 4',4'''-(phenazine-5,10-diyl)bis(([1,1'-biphenyl]-4-carbonitrile)) (**BPN**) the single-crystal diffraction data was collected using ω-scans on a Rigaku XtaLAB Synergy S four-circle diffractometer with a Hybrid Pixel Array Detector and a PhotonJet X-ray source for Cu-K_α radiation (λ = 1.54184 Å) with a multilayer mirror monochromator. The data were collected under a cold nitrogen gas-stream (Oxford Cryostream liquid nitrogen cooling system) at 140 K (**β-pBN**) or 100 K (**mBN**, **BPN**). Data reduction and absorption correction were performed with APEX2,[4] SAINT[5] and SADABS on the Bruker device and by CrysAlisPro on the Rigaku diffractometer [6]. Structures were solved by direct methods with SHELX-2018 and refined with full-matrix least squares refinements on F^2 using SHELXL [7] in OLEX2 [8]. Crystal data and details on the structure refinement are given in Table S1 and Table S2. All hydrogen atoms were positioned geometrically and refined using riding models with $U_{iso}(H) = 1.2 \cdot U_{eq}$. For structure **BPN** the chloroform solvent molecule was disordered over two positions and refined in a 66:34 ratio. Graphics were drawn with the program Diamond.[9]

Table S1. Crystal data and structure refinement for α- and β-polymorph of **pBN**.

	α-pBN reported previously [10]	**β-pBN** reported here
Identification code	wq_2_2	mo_th_dp_paralinker_0m_a
CCDC number	2156760	2238744
Empirical formula	$C_{26}H_{16}N_4$	$C_{26}H_{16}N_4$
Formula weight / g mol^{-1}	384.43	384.43
Temperature / K	149.99(10)	140.0(10)
Crystal system	Monoclinic	Triclinic
Space group	$P2_1$ (no. 4)	$P\bar{1}$ (no. 2)
a / Å	9.16980(10)	9.2154(7)
b / Å	25.87320(10)	9.8882(8)
c / Å	13.00690(10)	11.5256(9)
α / °	110.2310(10)°	105.439(4)
β / °	90	100.122(4)
γ / °	90	104.034(4)
Volume / Å^3	2895.53(4)	949.16(13)
Z	6	2
ρ_{calc} / g cm^{-3}	1.323	1.345
μ / mm^{-1}	0.630	0.082
F(000)	1200	400
Crystal size / mm^3	0.08 × 0.07 × 0.05	0.24 × 0.15 × 0.1
Radiation	Cu *Kα* (*λ* = 1.54184 Å)	Mo *Kα* (*λ* = 0.71073 Å)
2θ range for data collection / °	3.416 to 67.080	1.90 to 30.51
Index ranges	-10 ≤ *h*≤ 10, -30 ≤ *k* ≤ 30, -15 ≤ *l* ≤ 15	-13 ≤ *h* ≤ 13, -14 ≤ *k* ≤ 14, -16 ≤ *l* ≤ 16
Reflections collected	77636	19393
Independent reflections	10131 (R_{int} = 0.0284)	5723 (R_{int} = 0.0304)

Data/restraints/parameters	10131 / 1 / 812	5723 / 0 / 271
Final *R* indexes [$I \geq 2\sigma(I)$] [a]	R_1 = 0.0281, wR_2 = 0.0751	R_1 = 0.0508, wR_2 = 0.1257
Final *R* indexes [all data] [a]	R_1 = 0.0288, wR_2 = 0.0757	R_1 = 0.0760, wR_2 = 0.1398
Goodness-of-fit on F^2 [b]	1.043	1.060
Largest diff. peak/hole / e Å^{-3}	0.114 and -0.229	0.326 and -0.263
Absolute structure parameter	0.2(3)	

[a] Full-matrix least-square refinement on F^2 as implemented in SHELX. $R_1 = [\Sigma(\|F_o\| - |F_c|\|)/\Sigma|F_o|]$; $wR_2 = [\Sigma[w(F_o^2-F_c^2)^2]/\Sigma[w(F_o^2)^2]]^{1/2}$ where $w^{-1} = [\sigma^2(F_o^2) + (aP)^2 + bP]$, $P = [2F_c^2 + \mathrm{Max}(F_o^2, 0)] / 3$, *a* and *b* are refined parameters. [b] Goodness-of-fit $S = [\Sigma[w(F_o^2-F_c^2)^2]/(n-p)]^{1/2}$.

Table S2. Crystallographic details for structures **mBN** and **BPN** · $CHCl_3$.

	mBN	**BPN** · $CHCl_3$
Identification code	DP-metaLinker	DP-LinkerA2
CCDC number	2222499	2222500
Empirical formula	$C_{26}H_{16}N_4$	$C_{39}H_{25}Cl_3N_4$
Formula weight / g mol^{-1}	384.43	655.98
Temperature / K	100.0(1)	100.0(1)
Crystal system	monoclinic	triclinic
Space group	$P2_1/c$ (no. 14)	$P\bar{1}$ (no. 2)
a / Å	12.7220(4)	9.4403(2)
b / Å	7.6706(2)	12.0125(2)
c / Å	11.0125(3)	14.3830(3)
α / °	90	80.303(2)
β / °	113.828(4)	82.611(2)
γ / °	90	78.921(2)
Volume / Å^3	983.06(6)	1569.97(6)
Z	2	2
ρ_{calc} / g cm^{-3}	1.299	1.388
μ / mm^{-1}	0.618	2.922
F(000)	400.0	676.0
Crystal size / mm^3	0.64 × 0.39 × 0.2	0.18 × 0.06 × 0.04
Radiation	Cu *Kα* (*λ* = 1.54184 Å)	Cu *Kα* (*λ* = 1.54184 Å)
2θ range for data collection/°	3.798 to 78.680	3.133 to 79.754
Index ranges	-13 ≤ *h* ≤ 16, -9 ≤ *k* ≤ 7, -13 ≤ *l* ≤ 13	-12 ≤ *h* ≤ 11, -14 ≤ *k* ≤ 15, -17 ≤ *l* ≤ 17
Reflections collected	11223	45762
Independent reflections	2024 [R_{int} =0.0229, R_{sigma} = 0.0143]	6294 [R_{int} =0.0476, R_{sigma} = 0.0257]
Data/restraints/parameters	2024/0/136	6294/0/460
Final *R* indexes [$I \geq 2\sigma(I)$] [a]	R_1 = 0.0360, wR_2 = 0.0950	R_1 = 0.0418, wR_2 = 0.1000
Final *R* indexes [all data] [a]	R_1 = 0.0377, wR_2 = 0.0963	R_1 = 0.0526, wR_2 = 0.1037
Goodness-of-fit on F^2 [b]	1.047	1.057
Largest diff. peak/hole / e Å^{-3}	0.14/-0.21	0.20/-0.28

[a] Full-matrix least-square refinement on F^2 as implemented in SHELX. $R_1 = [\Sigma(\|F_o\| - |F_c|\|)/\Sigma|F_o|]$; $wR_2 = [\Sigma[w(F_o^2-F_c^2)^2]/\Sigma[w(F_o^2)^2]]^{1/2}$ where $w^{-1} = [\sigma^2(F_o^2) + (aP)^2 + bP]$, $P = [2F_c^2 + \mathrm{Max}(F_o^2, 0)] / 3$, *a* and *b* are refined parameters. [b] Goodness-of-fit $S = [\Sigma[w(F_o^2-F_c^2)^2]/(n-p)]^{1/2}$.

Comparison of α- and β-polymorph of pBN

Both polymorphs consist of two type of molecules, namely the ‘linear’ one and the ‘distorted one’ (ratios 1:1 in **β-pBN** and 1:2 in **α-pBN**), with a characteristic non-planarity of the latter associated with the weak, but clearly distinguishable, pyramidality of the N atoms (Table S3), constituting the dihydrophenazine core (Figure S1 and Figure 2 in the main text).

Table S3. Listing of angular distortions of the independent **pBN** molecules constituting the structures of the two known α- and β-polymorphs expressed as the sum of the C-N-C angles at the N atoms of the phenazinediyl core.

α-pBN (reported earlier)		**β-pBN** (reported here)	
Molecule 1, (‘linear’)	Σ(∠CNC) / ° [a]	Molecule 1, (linear)	Σ(∠CNC) / ° [a]
N(1)	360.0	N(1)	359.8
N(2)	359.3	N(2)	359.8
Molecule 2, (‘distorted’)	Σ(∠CNC) / ° [a,b]	Molecule 2, (‘distorted’)	Σ(∠CNC) / ° [a,b]
N(1)	356.5	N(1)	355.8
N(2)	358.7	N(2)	355.8
Molecule 3, (‘distorted’)	Σ(∠CNC), ° [a,b]		
N(1)	359.9 [a]		
N(2)	357.3		

[a] Σ(∠CNC) = ∠C1NC2 + ∠C2NC3 + ∠C3NC2, i.e. the sum of all angles between bonded atoms, with N atoms serving a vertex of the angles; a measure of non-planarity, with 360° corresponding to a planar case.

[b] Due to the significant distortion of the phenazine moiety the geometry of the N-atom environment is nearly planar, but the direction of the N-C_{Ph} bond is still significantly off the least squares plane for atoms constituting the phenazinediyl plane, *i.e.* the molecule is notwithstanding characteristically non-linear.

The α- and β-polymorphs could be rationalized as being both constituted from layers of molecules of the same type, following the ABBABB… and ABAB… patterns (Figure S1a,b), where A and B are the layers consisting of ‘linear’ and ‘disordered’ molecules, respectively only. The packing efficiency is only slightly better in the β-polymorph compared to the α-polymorph, with the respective densities being 1.345 vs. 1.323 g cm^{-3} (Table S1).

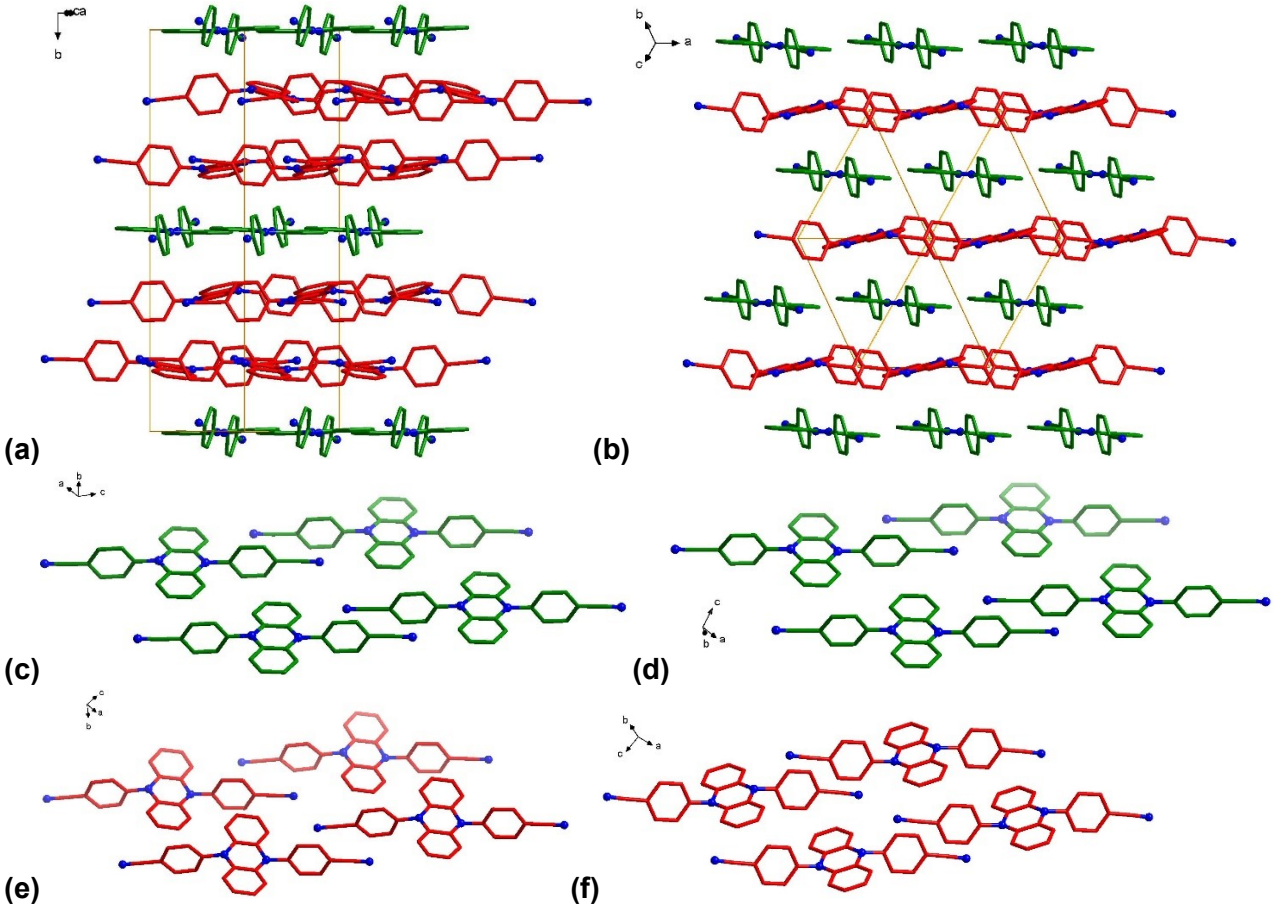

Figure S1. Comparison of the packing diagrams in the structures of **pBN**.
The previously reported polymorph **α-pBN** [10] (monoclinic, $P2_1$ (no. 4), Z' = 3; crystallization by slow evaporation of a hexane/dichloromethane solution) left panes: **(a)**, **(c)**, **(e)**.

The **β-pBN** reported here (triclinic, $P\bar{1}$ (no. 2), Z' = 1; crystallization by slow evaporation of a solution in $CHCl_3$) right panes: **(b)**, **(d)**, **(f)**.
The linear molecules are depicted in green, the distorted ones in red.

S4 Supramolecular interaction analysis

The supramolecular packing interactions have been analyzed for compounds **β-pBN**, **mBN** and **BPN** with PLATON.[11,12,13]
The PLATON-listing "Analysis of Short Ring-Interactions" for possible π-stacking interactions yielded no π-π-stacking interactions in **β-pBN** or **mBN** and only one in **BPN**. π-Stacking, especially significant π-stacking would mean rather short centroid-centroid contacts (< 3.8 Å), near parallel ring planes (α < 10° to ~ 0° or even exactly 0° by symmetry), small slip angles (β, γ < 25°) and vertical displacements (slippage < 1.5 Å) which translate into a sizable overlap of the aryl-plane areas (Scheme S1).[14,15]

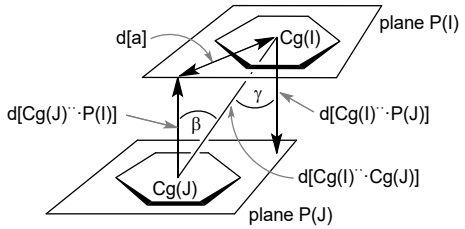

Scheme S1. Graphical presentation of the parameters used for the description of π-π stacking.

However, from the "Analysis of X-H...Cg(Pi-Ring) Interactions (H..Cg < 3.0 Å – γ< 30.0°) significant intermolecular C-H···π contacts were found in **mBN**, which start around 2.57 Å for the (C-)H···ring centroid distances with H-perp starting below 2.5 Å and C-H··Cg > 135° (Scheme S2) [16].

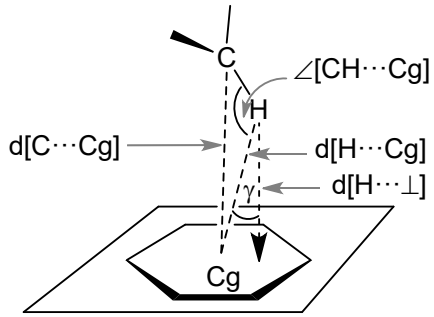

Scheme S2. Graphical presentation of the parameters used for the description of CH-π interactions.

Furthermore, there are C-H···N contacts in the solid-state packing arrangements of all three compounds.

Compound β-pBN:

Figure S2 gives an approximate view along the N···N axis in **β-pBN** to illustrate the planar nature of the pyrazine ring in both the linear and distorted molecule of **β-pBN** and shows the packing diagram.

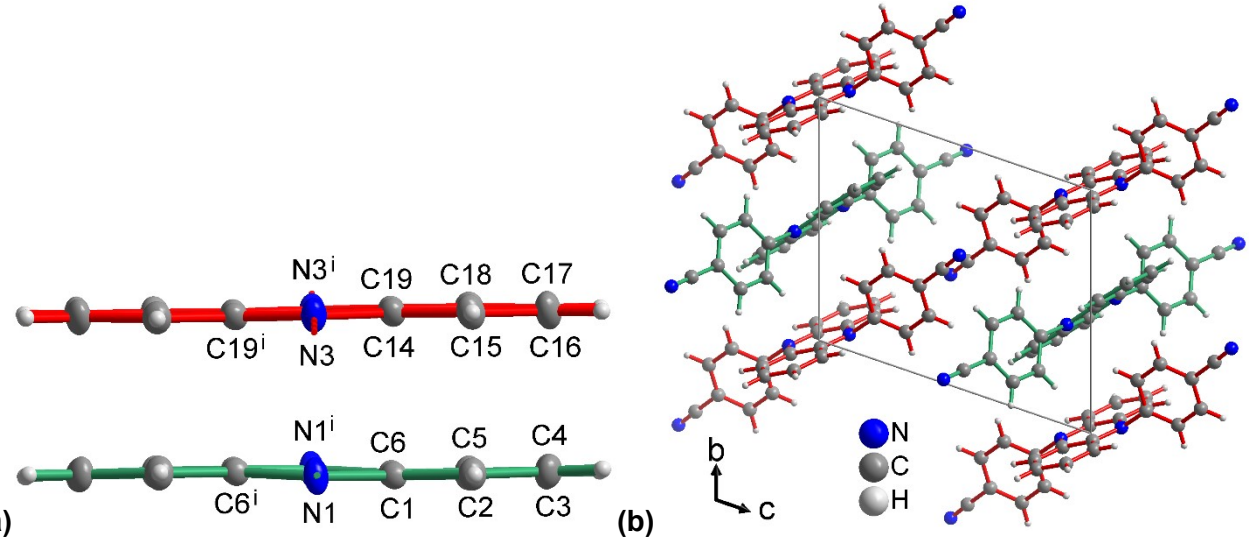

Figure S2. (a) Approximate view along the N···N axis in the linear (green) and distorted (red) molecules of **β-pBN** and **(b)** packing diagram. The linear molecules are depicted with green bonds, the distorted ones with red bonds.

Intermolecular C-H···π contacts in the packing of **β-pBN** (shown in Figure S3):

Analysis of X-H...Cg(Pi-Ring) Interactions (H..Cg < 3.0 Ang. - Gamma < 30.0 Deg)

==========- Cg(J) = Center of gravity of ring J (Plane number above)
- H-Perp = Perpendicular distance of H to ring plane J
- Gamma = Angle between Cg-H vector and ring J normal
- X-H..Cg = X-H-Cg angle (degrees)
- X..Cg = Distance of X to Cg (Angstrom)
- X-H, Pi = Angle of the X-H bond with the Pi-plane (i.e.' Perpendicular = 90 degrees, Parallel = 0 degrees)

X--H(I)	Res(I)	Cg(J) [ARU(J)]	H..Cg	H-Perp	Gamma	X-H..Cg	X..Cg	X-H,Pi
C4 -H4	[1] -> Cg3	[1455.01]	2.85	2.83	7.02	154	3.7317(18)	59
C12 -H12	[1] -> Cg8	[2676.02]	2.89	2.84	10.84	145	3.7073(17)	63
C21 -H21	[2] -> Cg1	[2666.01]	2.64	2.55	14.71	138	3.4020(17)	56

C21	-H21	[2] -> Cg4	[2666.01]	2.80	2.55	24.51	120	3.3799(17)	55
C21	-H21	[2] -> Cg6	[2666.01]	2.64	2.55	14.36	138	3.4020(16)	54
C22	-H22	[2] -> Cg2	[2666.01]	2.50	2.50	3.24	144	3.3203(17)	58
C22	-H22	[2] -> Cg4	[2666.01]	2.81	2.49	27.47	119	3.3798(16)	57

[1455] = -1+X,Y,Z
[2676] = 1-X,2-Y,1-Z
[2666] = 1-X,1-Y,1-Z

Cg(1) = centroid of N1-C1-C6-N1i-C1i-C6i
Cg(2) = centroid of C1-C2-C3-C4-C5-C6
Cg(3) = centroid of C7-C8-C9-C10-C11-C12
Cg(4) = centroid of N1-C1-C2-C3-C4-C5-C6-N1i-C1i-C6i
Cg(6) = centroid of N1-C1-C2-C3-C4-C5-C6-N1i-C1i-C2i-C3i-C4i-C5i-C6i = corresponds to Cg(1)
Cg(8) = centroid of C14-C15-C16-C17-C18-C19

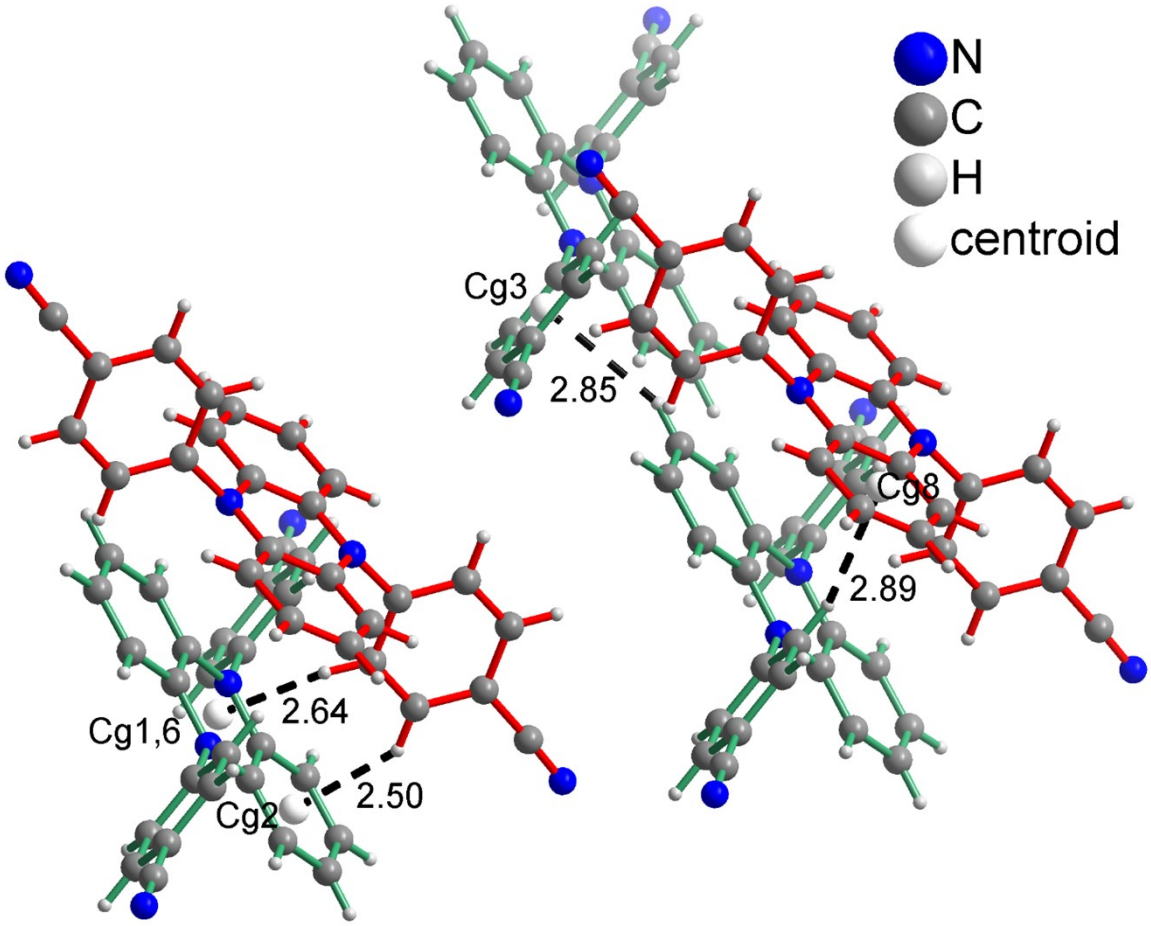

Figure S3. Intermolecular C-H···π contacts in **β-pBN**. Cg = ring centroids and distances (in Å) according to the Table above. The linear molecules are depicted with green bonds, the distorted ones with red bonds.

Intermolecular C-H···N contacts in the packing of **β-pBN** (shown in Figure S4)

Analysis of Potential Hydrogen Bonds and Schemes with d(D...A) < R(D)+R(A)+0.50, d(H...A) < R(H)+R(A)-0.12 Ang., D-H...A > 100.0 Deg

Nr	Typ	Res	Donor	--- H....Acceptor [	ARU]	D - H	H...A	D...A	D - H...A
1	1	C2	--H2	..N2	[2776.01]	0.95	2.55	3.363(2)	143
2	2	C15	--H15	..N4	[2666.02]	0.95	2.59	3.441(2)	150

[2776.] = [2_776] = 2-x,2-y,1-z
[2666.] = [2_666] = 1-x,1-y,1-z

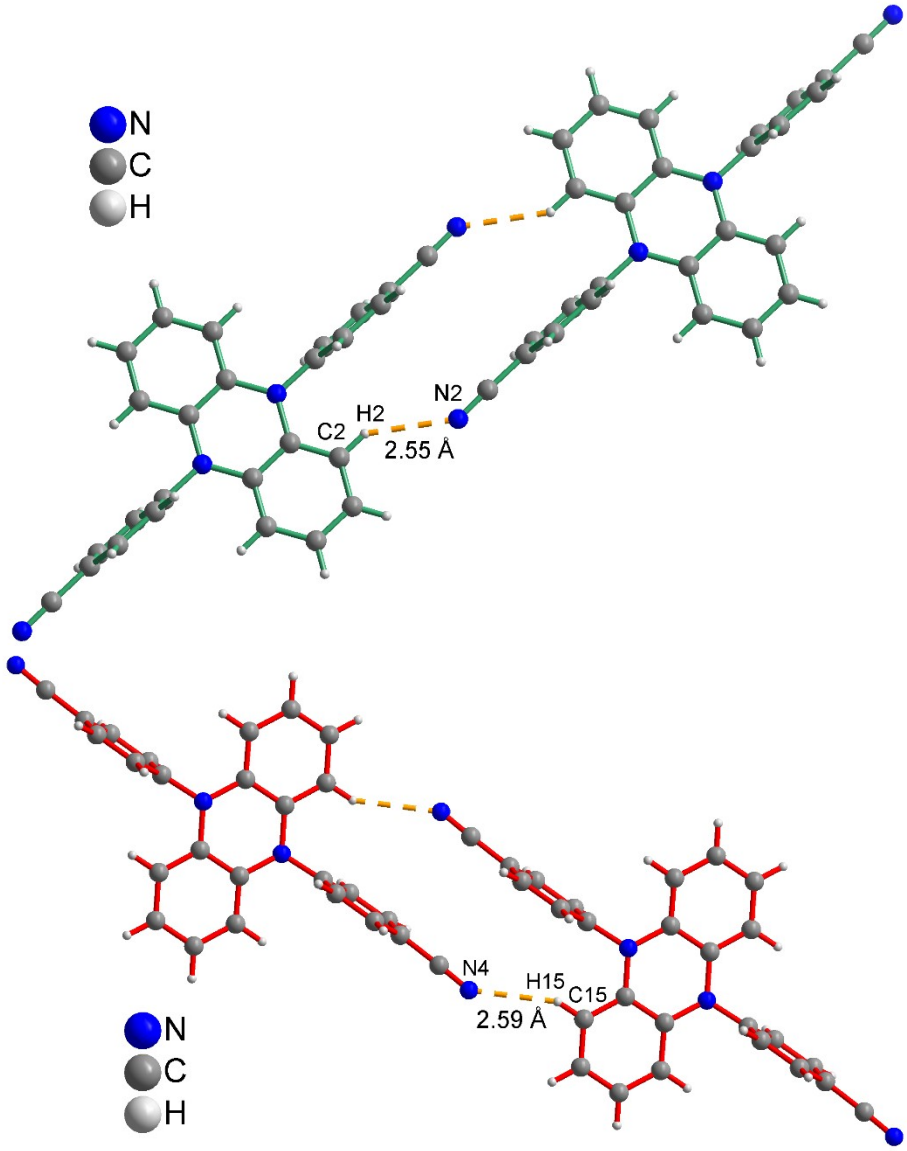

Figure S4. Intermolecular C-H·· N contacts in **β-pBN** according to the Table above. The linear molecules are depicted with green bonds, the distorted ones with red bonds.

Compound mBN:

Figure S5 gives an approximate view along the N···N axis in **mBN** to illustrate the planar nature of the pyrazine ring in **mBN** and shows the packing diagram.

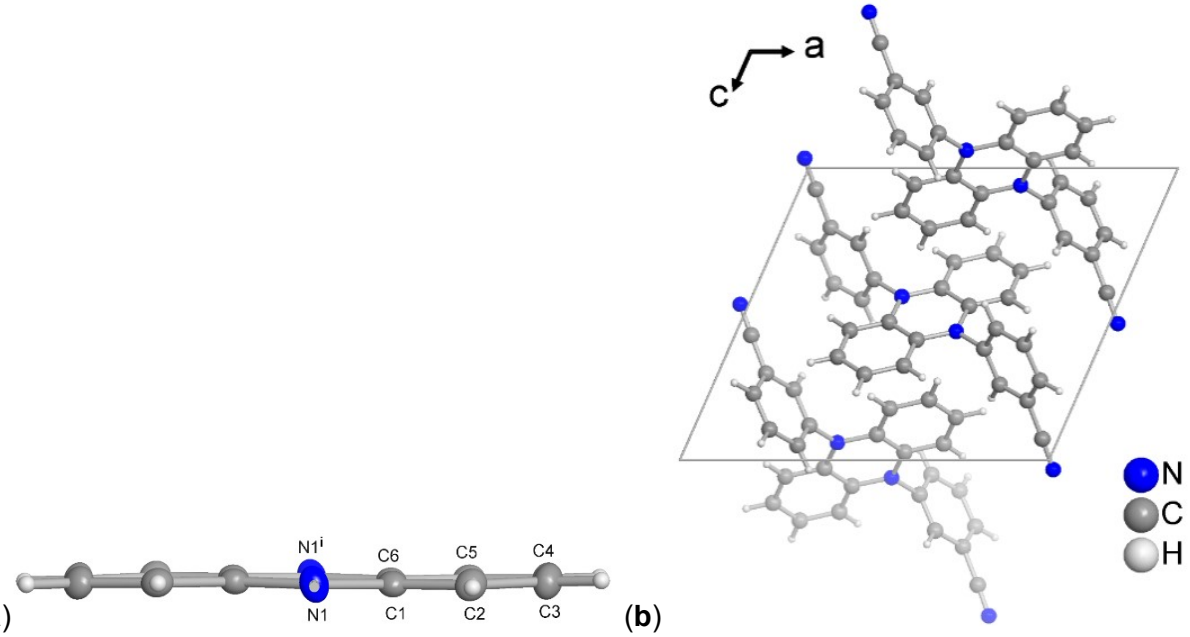

(**a**) (**b**)

Figure S5. (**a**) Approximate view along the N···N axis in **mBN** and (**b**) packing diagram.

Intermolecular C-H···π contacts in the packing of **mBN** (shown in Figure S6):

Analysis of X-H...Cg(Pi-Ring) Interactions (H..Cg < 3.0 Ang. - Gamma < 30.0 Deg)

==========- Cg(J)

= Center of gravity of ring J (Plane number above)
- H-Perp = Perpendicular distance of H to ring plane J
- Gamma = Angle between Cg-H vector and ring J normal
- X-H..Cg = X-H-Cg angle (degrees)
- X..Cg = Distance of X to Cg (Angstrom)
- X-H, Pi = Angle of the X-H bond with the Pi-plane (i.e.' Perpendicular = 90 degrees, Parallel = 0 degrees)

X--H(I)	Res(I)	Cg(J)	[ARU(J)]	H..Cg	H-Perp	Gamma	X-H..Cg	X..Cg	X-H,Pi
C(2) -H(2)	[1] ->	Cg(2)	[2656.01]	2.95	2.82	16.89	135	3.6779(11)	52
C(3) -H(3)	[1] ->	Cg(1)	[2656.01]	2.57	2.49	15.07	148	3.4194(12)	67
C(3) -H(3)	[1] ->	Cg(4)	[2656.01]	2.66	2.48	21.65	136	3.4142(11)	67
C(3) -H(3)	[1] ->	Cg(6)	[2656.01]	2.57	2.48	15.80	148	3.4194(11)	67

[2656] = 1-X,1/2+Y,3/2-Z
[4554] = X,1/2-Y,-1/2+Z

Cg(1) = centroid of N1-C1-C6-N1i-C1i-C6i
Cg(2) = centroid of C1-C2-C3-C4-C5-C6
Cg(4) = centroid of N1-C1-C2-C3-C4-C5-C6-N1i-C1i-C6i
Cg(6) = centroid of N1-C1-C2-C3-C4-C5-C6- N1i-C1i-C2i-C3i-C4i-C5i-C6i = corresponds to Cg(1)

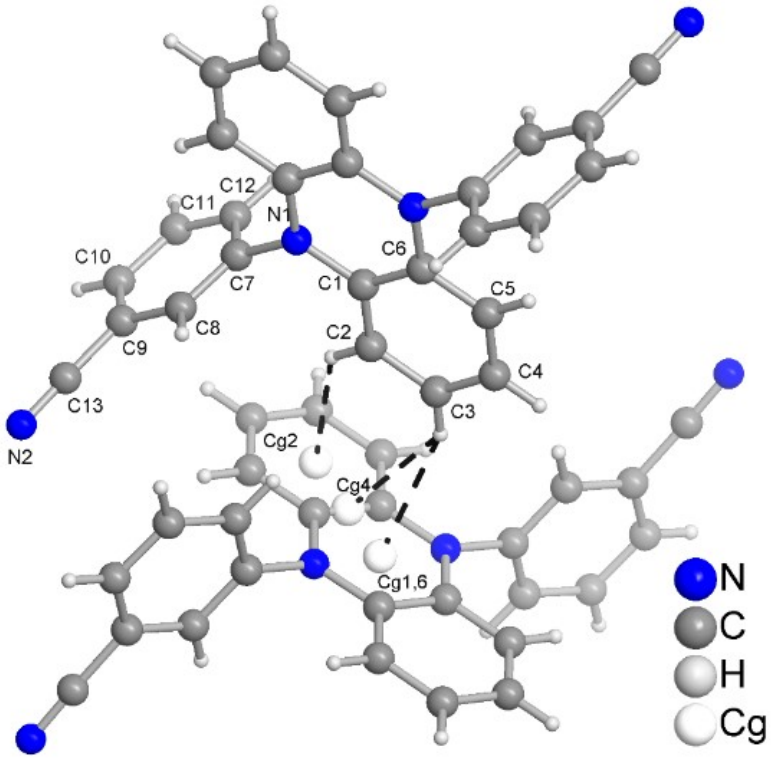

Figure S6. Intermolecular C-H···π contacts in **mBN**. Symmetry transformation i = –*x*+1, –*y*, –*z*+2. Cg = ring centroids according to the Table above.

Intermolecular C-H···N contacts in the packing of **mBN** (shown in Figure S7)

Analysis of Potential Hydrogen Bonds and Schemes with d(D...A) < R(D)+R(A)+0.50, d(H...A) < R(H)+R(A)-0.12 Ang., D-H...A > 100.0 Deg

Nr	Typ	Res	Donor	---	H....Acceptor	[ARU]	D - H	H...A	D...A	D - H...A
1	1	C(4)	--H(4)	..	N(2)	[4655.01]	0.95	2.61	3.3597(17)	136

[4655.] = [4_666] = 1+x,1/2-y,1/2+z

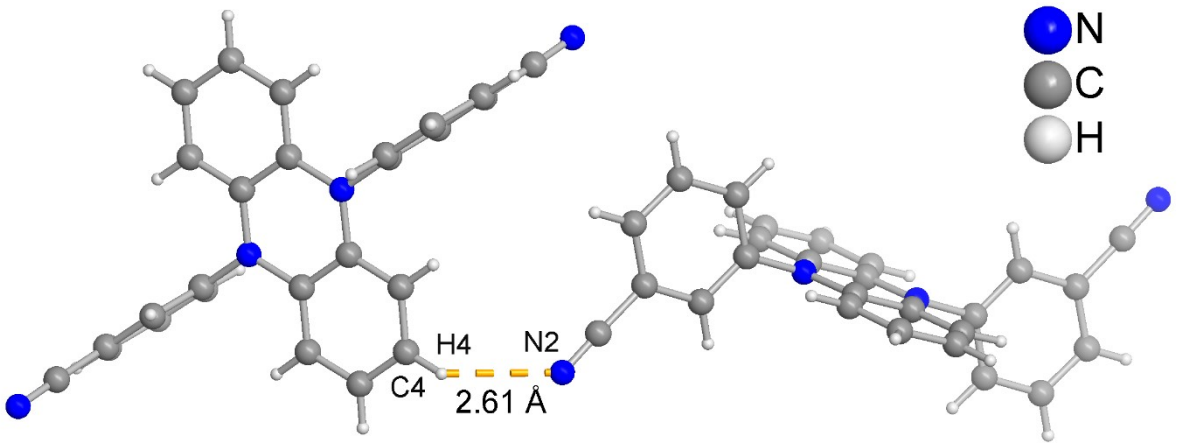

Figure S7. Intermolecular C-H·· N contact in **mBN** according to the Table above.

Compound BPN:

Figure S8 depicts the molecular structure of **BPN** with the chloroform solvent of crystallization, gives an approximate view along the N···N axis in **BPN** to illustrate the bending and shows the packing diagram.

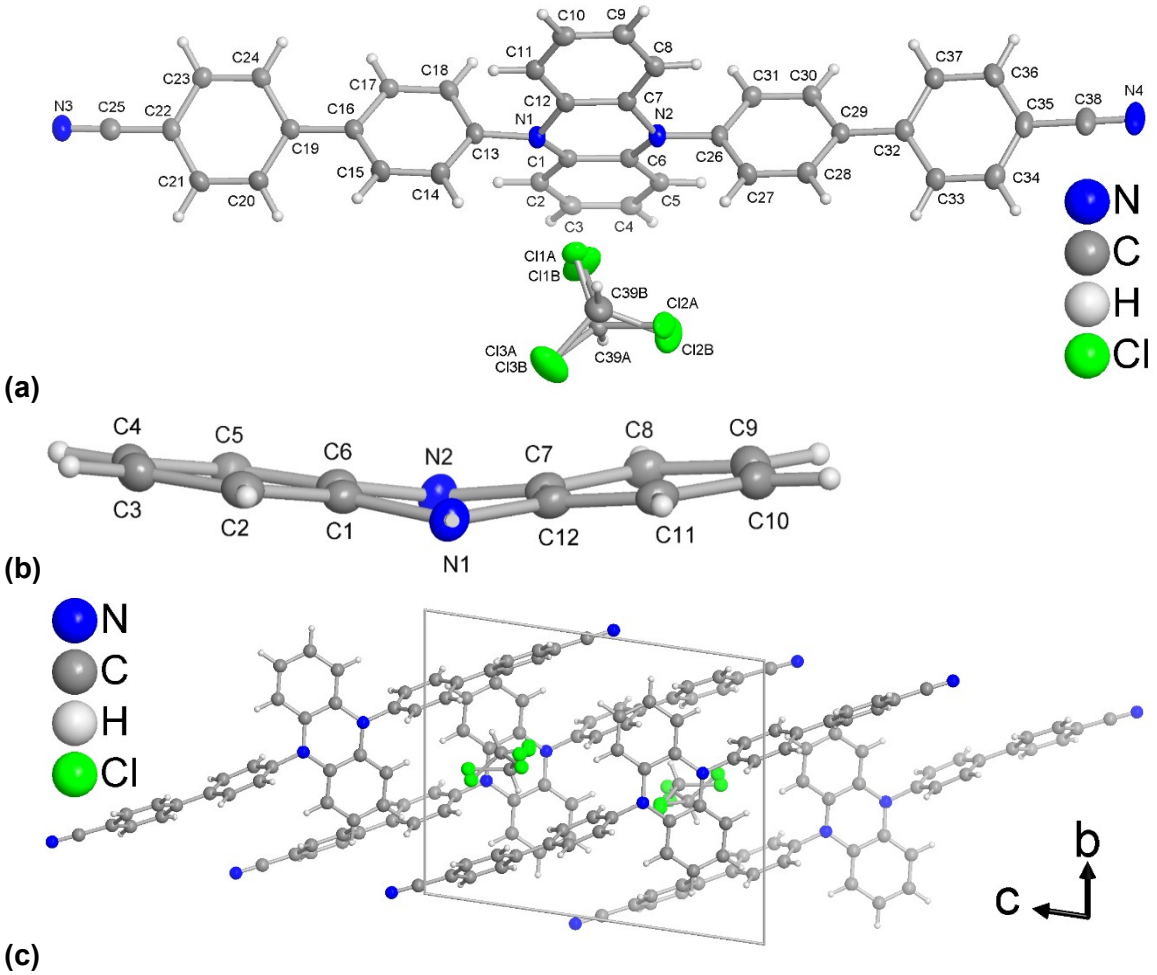

Figure S8. (a) Molecular structure of **BPN** showing also the disordered $CHCl_3$ solvent molecule in the crystalline state (50% thermal ellipsoids, H atoms with arbitrary radii). **(b)** Approximate view along the N···N axis in **BPN** to illustrate the bending by 16.00° of the two pyrazine halves in **BPN**. The angles in **BPN** between the benzene ring planes and the anellated half of the pyrazine ring are 2.71° (C1-C6) and 1.19° (C7-C12). **(c)** Section of the packing diagram.

Intermolecular π–π-Stacking interactions in the packing of **BPN** (shown in Figure S9a):

==========

Analysis of Short Ring-Interactions with Cg-Cg Distances < 6.0 Ang., Alpha < 20.000 Deg. and Beta < 60.0 Deg.

==========

- Cg(I) = Plane number I (= ring number in () above)
- Alpha = Dihedral Angle between Planes I and J (Deg)
- Beta = Angle Cg(I)-->Cg(J) or Cg(I)-->Me vector and normal to plane I (Deg)
- Gamma = Angle Cg(I)-->Cg(J) vector and normal to plane J (Deg)
- Cg-Cg = Distance between ring Centroids (Ang.)
- CgI_Perp = Perpendicular distance of Cg(I) on ring J (Ang.)
- CgJ_Perp = Perpendicular distance of Cg(J) on ring I (Ang.)
- Slippage = Distance between Cg(I) and Perpendicular Projection of Cg(J) on Ring I (Ang).
- P,Q,R,S = J-Plane Parameters for Carth. Coord. (Xo, Yo, Zo)

Cg(I)	Res(I)	Cg(J)	[ARU(J)]	Cg-Cg	Alpha	Beta	Gamma	CgI_Perp	CgJ_Perp	Slippage
Cg(5)	[1] ->	Cg(7)	[1564.01]	3.7043(10)	5.87(8)	28.3	22.4	3.4247(7)	3.2626(7)	1.754
Cg(7)	[1] ->	Cg(5)	[1546.01]	3.7041(10)	5.87(8)	22.4	28.3	3.2625(7)	3.4246(7)	1.412

(Cg-Cg contacts above 4.9 Å have been omitted.)

[1564] = X,1+Y,-1+Z
[1546] = X,-1+Y,1+Z
Cg(5) = centroid of C19-C20-C21-C22-C23-C24
Cg(7) = centroid of C32-C33-C34-C35-C36-C37

Intermolecular C-H···π contacts in the packing of **BPN** (shown in Figure S9b):

Analysis of X-H...Cg(Pi-Ring) Interactions (H..Cg < 3.0 Ang. - Gamma < 30.0 Deg)

==========- Cg(J) = Center of gravity of ring J (Plane number above)
- H-Perp = Perpendicular distance of H to ring plane J
- Gamma = Angle between Cg-H vector and ring J normal
- X-H..Cg = X-H-Cg angle (degrees)
- X..Cg = Distance of X to Cg (Angstrom)
- X-H, Pi = Angle of the X-H bond with the Pi-plane (i.e.' Perpendicular = 90 degrees, Parallel = 0 degrees)

X--H(I)	Res(I)	Cg(J)	[ARU(J)]	H..Cg	H-Perp	Gamma	X-H..Cg	X..Cg	X-H,Pi
C(17) -H(17)	[1] ->	Cg(2)	[2666.01]	2.71	2.69	6.49	154	3.5831(18)	62
C(28) -H(28)	[1] ->	Cg(3)	[2567.01]	2.80	2.68	17.19	169	3.7406(19)	64

[2666] = 1-X,1-Y,1-Z
[2567] = -X,1-Y,2-Z

Cg(2) = centroid of C1-C2-C3-C4-C5-C6
Cg(3) = centroid of C7-C8-C9-C10-C11-C12

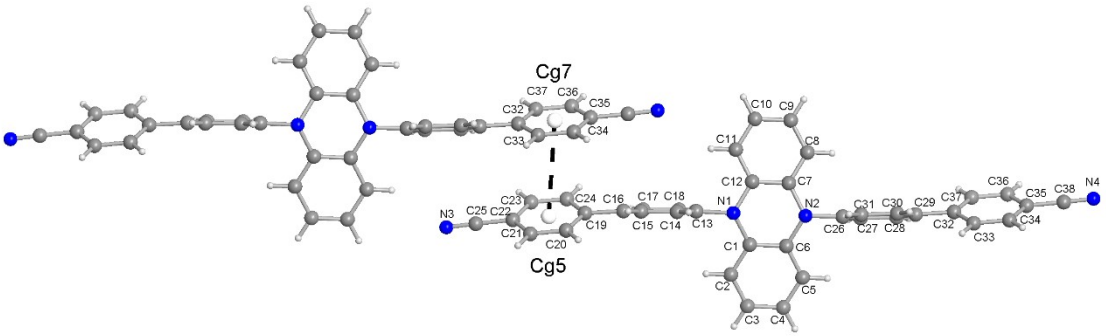

(a)

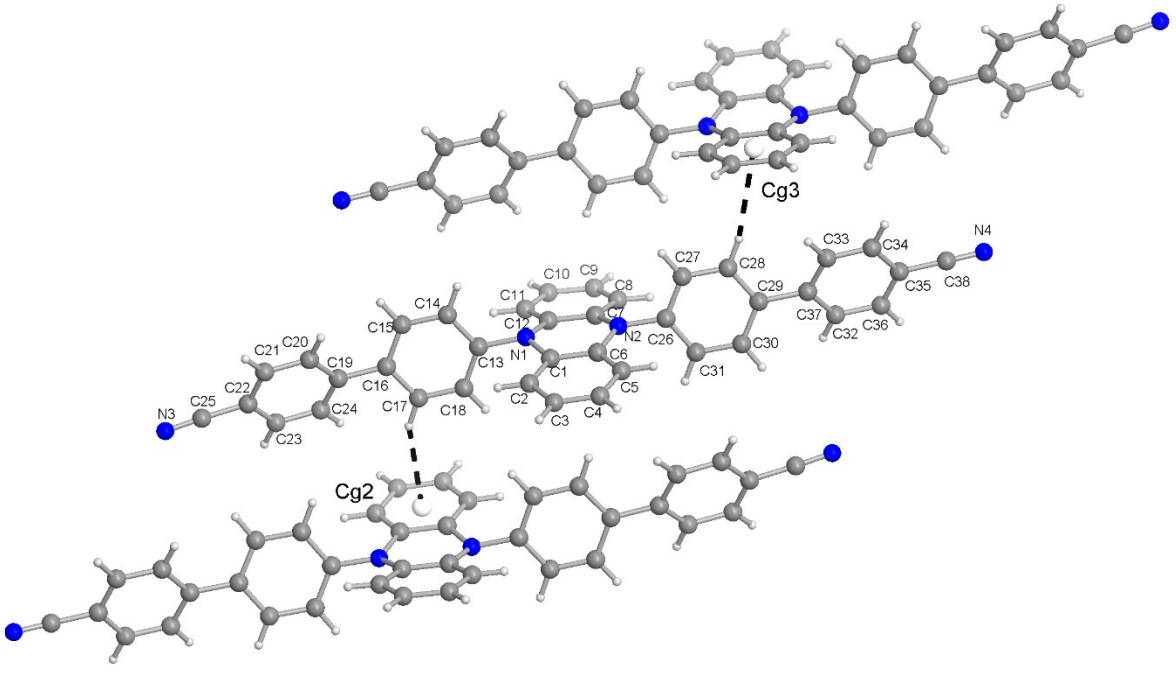

(b)

Figure S9. (a) π–π-Stacking interactions and **(b)** intermolecular C-H···π contacts in **BPN**. Cg = ring centroids according to the Table above.

Intermolecular C-H···N contacts in the packing of **BPN** (shown in Figure S10)

Analysis of Potential Hydrogen Bonds and Schemes with d(D...A) < R(D)+R(A)+0.50, d(H...A) < R(H)+R(A)-0.12 Ang., D-H...A > 100.0 Deg

Nr	Typ	Res	Donor --- H....Acceptor	[ARU]	D - H	H...A	D...A	D - H...A
1		1	C(5) --H(5) ..N(3)	[1546.01]	0.95	2.55	3.395(2)	149
3		1	C(11) --H(11) ..N(4)	[1564.01]	0.95	2.53	3.365(2)	147

[1564.] = [1_564] = x,1+y,-1+z
[1546.] = [1_546] = x,-1+y,1+z

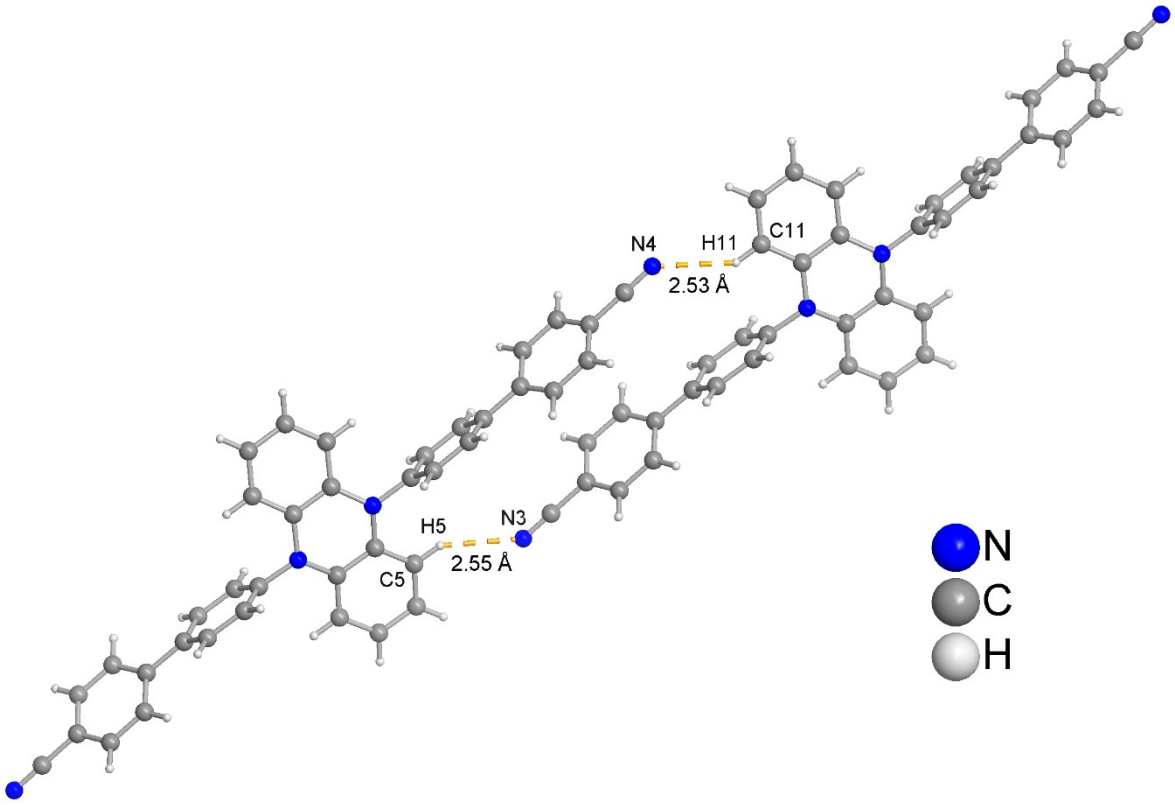

Figure S10. Intermolecular C-H·· N contacts in **BPN** according to the Table above.

S5 Photophysical properties

Emission spectra (Solid state)

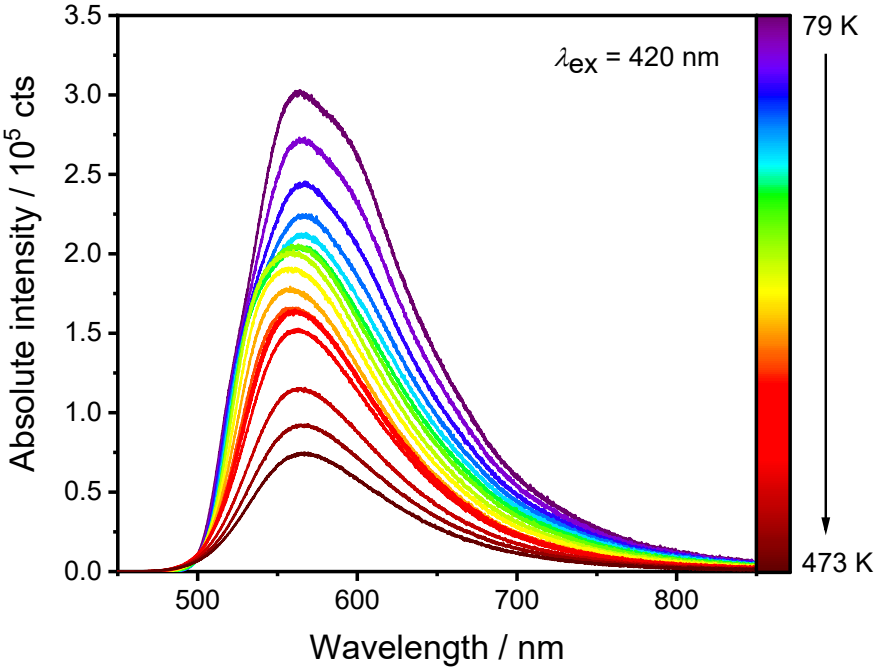

Figure S11. Temperature-dependent emission spectrum of powdered **pBN**. Excitation wavelength is indicated. Temperature intervals were ΔT = 25 K.

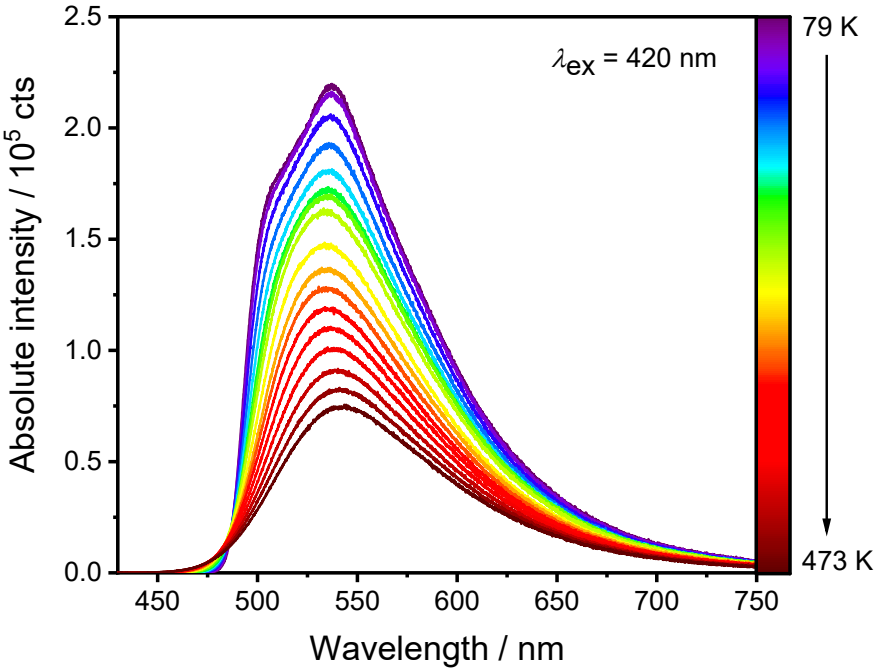

Figure S12. Temperature-dependent emission spectrum of powdered **mBN**. Excitation wavelength is indicated. Temperature intervals were ΔT = 25 K.

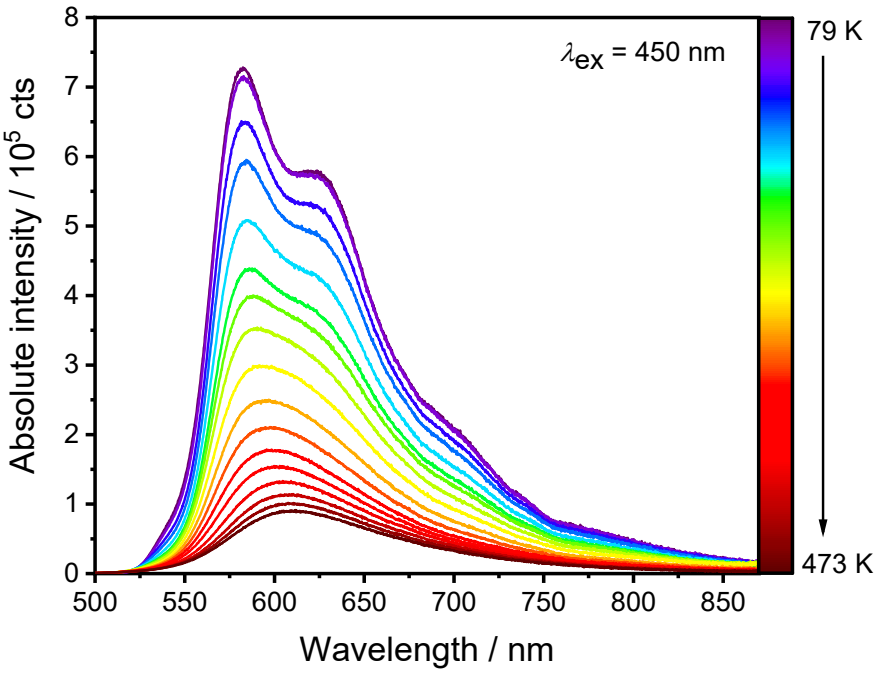

Figure S13. Temperature-dependent emission spectrum of powdered **BPN**. Excitation wavelength is indicated. Temperature intervals were ΔT = 25 K.

Arrhenius plots (Solid state)

The temperature-dependent delayed components were fitted to an Arrhenius law in the low temperature range:

$$k_{delayed}(T) = k_{d0}\exp\left(-\frac{\Delta E_{ST}}{k_B T}\right) \quad (1)$$

with k_{d0} as a pre-factor, ΔE_{ST} as the effective singlet-triplet energy gap, k_B as the Boltzmann constant and T as the absolute temperature. In the cases of **pBN** and **mBN**, the prompt and delayed components were obtained from the time-resolved luminescence by biexponential fits over the whole dynamic range,

$$I(t,T) = A_{prompt}\exp\left(-k_{prompt}(T)\cdot t\right) + A_{delayed}\exp\left(-k_{delayed}(T)\cdot t\right) \quad (2)$$

with $I(t, T)$ as the time-dependent intensity at a given temperature T, A_{prompt} and $A_{delayed}$ as the amplitudes of the prompt and delayed component, respectively, and $k_{prompt}(T)$ and $k_{delayed}(T)$ as the (eventually temperature-dependent) decay rate constants of the prompt and delayed fluorescence, respectively.

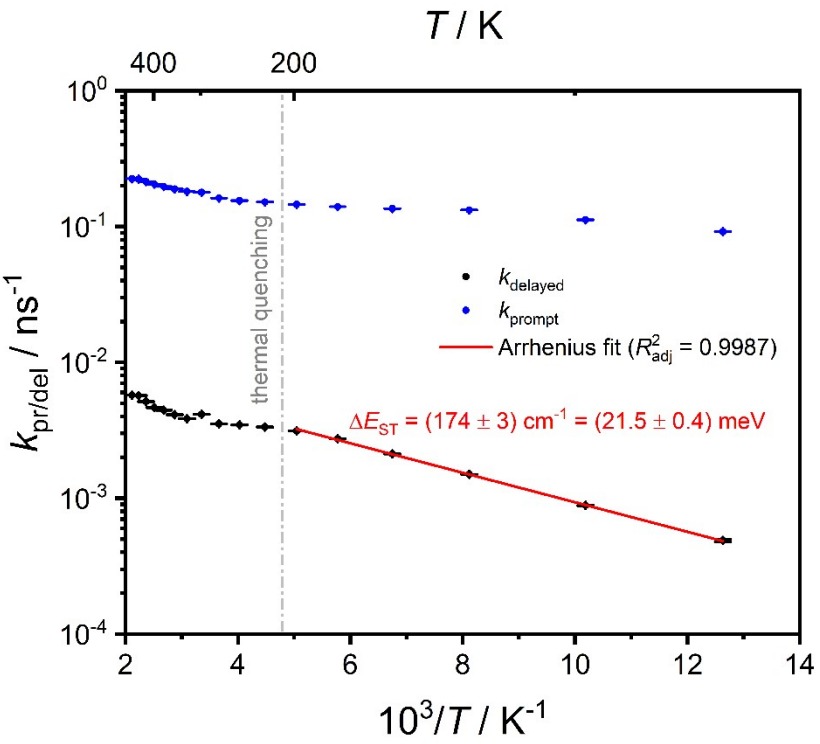

Figure S14. Arrhenius plot of the temperature-dependent time-resolved luminescence data of **pBN**.

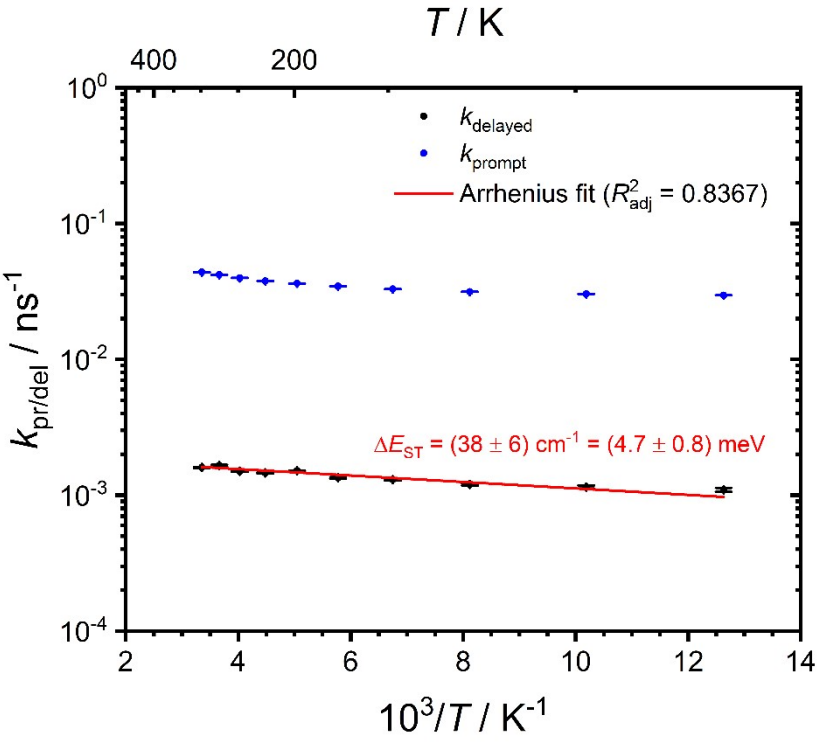

Figure S15. Arrhenius plot of the temperature-dependent time-resolved luminescence data of **mBN**.

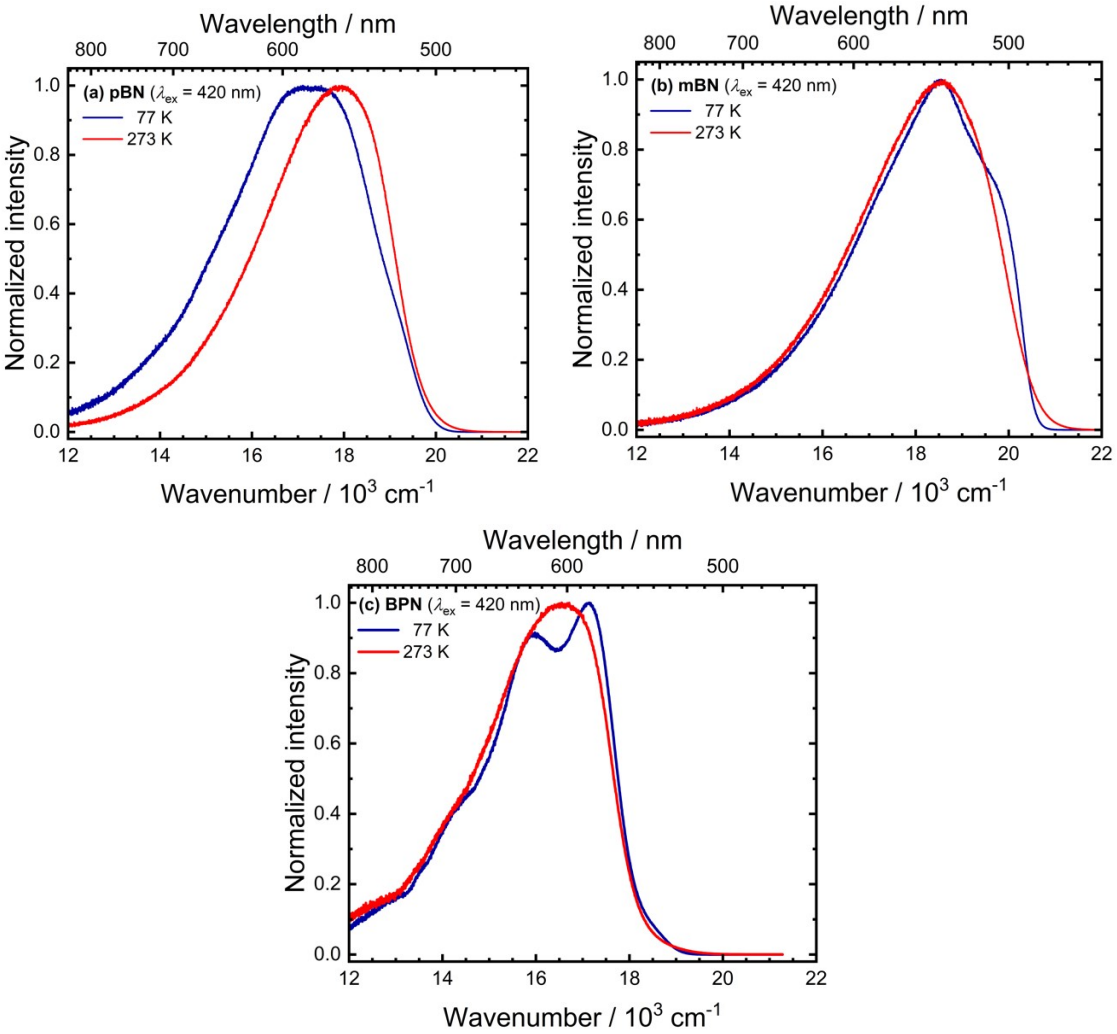

Figure S16. Photoluminescence spectra in wavenumber scale (including Jacobian λ^2 intensity correction) for **(a) pBN**, **(b) mBN**, and **(c) BPN** at 77 K (blue) and 273 K (red).

Absorption and emission spectra (solution state)

Compound pBN:

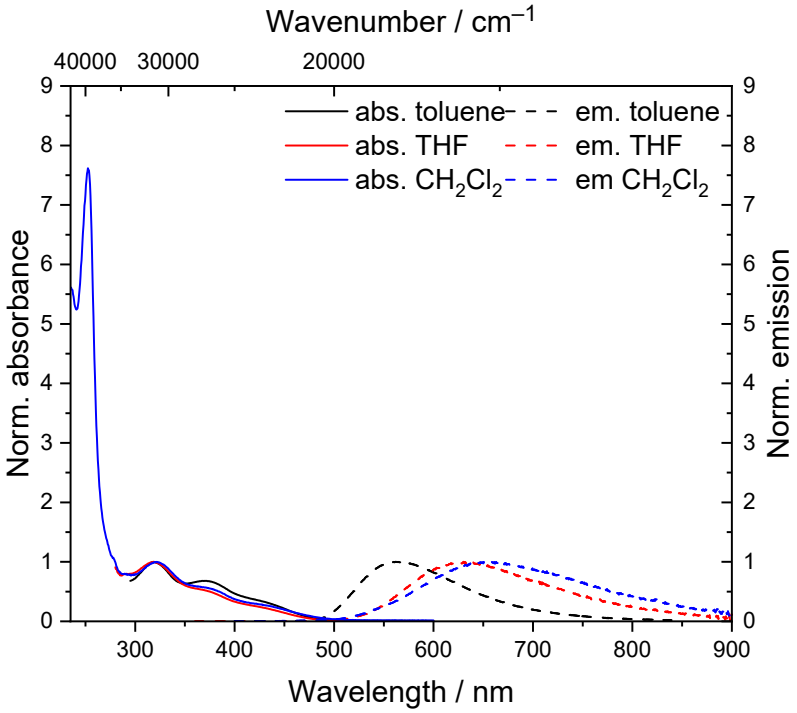

Figure S17. Absorbance and emission spectra of **pBN** recorded in solvents with different polarity (c = 10^{-5} mol/L, T = 293 K).

Compound **pBN** possesses in toluene (318 nm, ε = 2700 L mol^{-1} cm^{-1}), THF (318 nm, ε = 7200 L mol^{-1} cm^{-1}) and dichloromethane (321 nm, ε = 7700 L mol^{-1} cm^{-1}) one distinct absorption maximum, which is accompanied by two shoulders around 370 nm and 427 nm with weaker intensity (Figure S17, Table 1). In dichloromethane a maximum at higher energy at 255 nm with a molar absorption coefficient of 42600 L mol^{-1} cm^{-1} is detected (Table 1).

While the absorbance spectra are almost indifferent to the change of solvent polarity regarding their absorption maxima, the emission is strongly affected by solvent polarity and a distinct positive emission solvatochromicity can be observed in solvents of higher polarity (Table 1).[17] The broad emission bands (full width at half maximum (FWHM) from 3624 cm^{-1} (0.45 eV) to 4426 cm^{-1} (0.55 eV) are redshifted from toluene (562 nm) over THF (634 nm) to dichloromethane (659 nm) and a pronounced increase of the Stokes shifts from 9200 to 16000 cm^{-1} can be determined. The bathochromic emission shift with increasing solvent polarity indicates a significant charge transfer character of the excited state. CIE coordinates reveal yellow to orange emission colors (Figure S18). Emission is not intense and hardly visible to the eye in THF and dichloromethane. Luminescence lifetimes are in a typical range for organic chromophores[18], and decrease with increasing solvent polarity from toluene (τ = 5.7 ns) over THF (τ = 2.5 ns) to dichloromethane (τ = 1.0 ns). This observation indicates high non-radiative rate constants in each solvent.

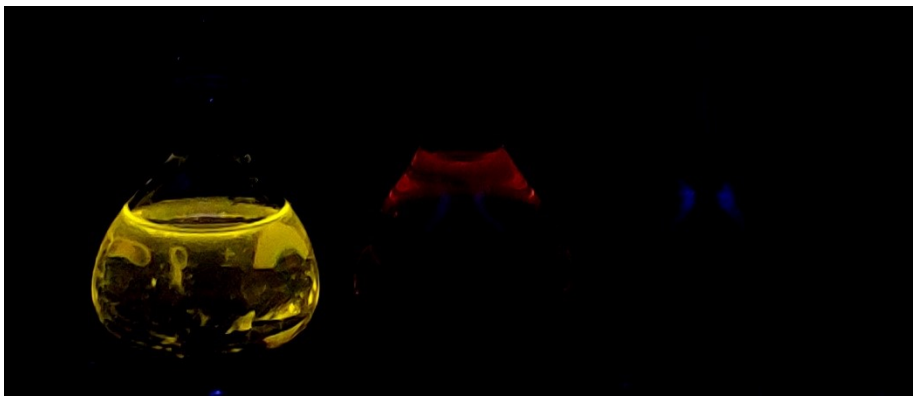

Figure S18. Emission of **pBN** in toluene, THF and dichloromethane (from left to right) (c = 10^{-4} mol/L, λ_{exc} = 365 nm).

Compound mBN:

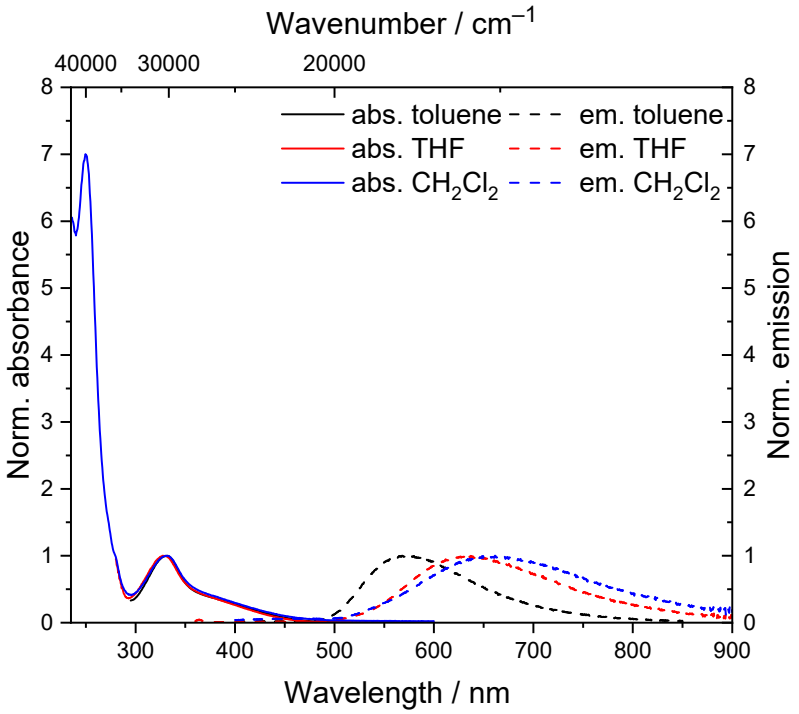

Figure S19. Absorbance and emission spectra of **mBN** recorded in solvents with different polarity (c = 10^{-5} mol/L, T = 293 K).

Compound **mBN** possesses in toluene (331 nm, ε = 6800 L mol^{-1} cm^{-1}) and THF (329 nm, ε = 5900 L mol^{-1} cm^{-1}) a distinct longest wavelength absorption maximum that is accompanied by broad tailing shoulder around 380 nm with weaker intensity (Figure S19, Table 1). In dichloromethane, the higher energy absorption band at 250 nm with a molar absorption coefficient of 54200 L mol^{-1} cm^{-1} is found (Table 1). Also, in dichloromethane a shoulder around 380 nm can be identified.

While the absorption spectra are almost indifferent to the change of solvent polarity, the emission is strongly affected by solvent polarity and a distinct positive emission solvatochromism can be

observed in solvents of higher polarity (Table 1).[17] The broad emission bands (full width at half maximum (FWHM) from 3746 cm^{-1} (0.47 eV) to 4517 cm^{-1} (0.56 eV) are redshifted from toluene (572 nm) over THF (634 nm) to dichloromethane (662 nm) and a pronounced increase of the Stokes shifts from 12700 to 15000 cm^{-1} can be determined. The bathochromic emission shift with increasing solvent polarity indicates a significant charge transfer character of the excited state. CIE coordinates indicate an orangish-yellow color in emission (Figure S20, Table 1). Emission intensity strongly decreases with increasing solvent polarity. Already in toluene the emission is very weak, being not visible to the eye in THF and dichloromethane (Figure S20). Furthermore, the luminescence lifetimes fall into the typical range for organic chromophores,[18] and the lifetimes decrease from toluene (τ = 8.9 ns) over THF (τ = 1.7 ns) to dichloromethane (τ = 1.6 ns). These observations indicate high non-radiative rate constants in each solvent.

Figure S20. Emission of **mBN** in toluene, THF and dichloromethane (from left to right) (c = 10^{-4} mol/L, λ_{exc} = 365 nm).

Compound BPN:

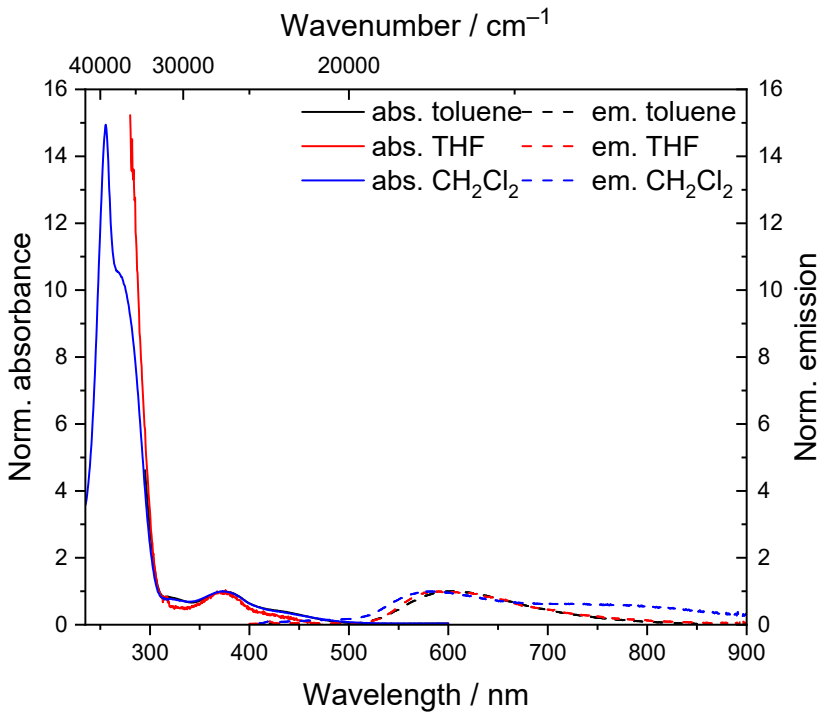

Figure S21. Absorbance and emission spectra of **BPN** recorded in solvents with different polarity (c = 10^{-5} mol/L, T = 293 K).

Compound **BPN** possesses in toluene (375 nm, ε = 6600 L mol^{-1} cm^{-1}) and THF (373 nm, ε = 1900 L mol^{-1} cm^{-1}) a distinct longest wavelength absorption maximum that is accompanied by tailing shoulder around 427 nm with weaker intensity (Figure S21, Table 1). In dichloromethane, the higher energy absorption band at 255 nm with a molar absorption coefficient of 98000 L mol^{-1} cm^{-1} is found (Table 1). Also, in dichloromethane a shoulder around 427 nm and 271 nm can be identified.

While the absorbance spectra are almost indifferent to the change of solvent polarity, the emission is strongly affected by solvent polarity and a distinct negative emission solvatochromism can be observed in solvents of higher polarity (Table 1).[17] The broad emission bands (full width at half maximum (FWHM) from 3564 cm^{-1} (0.44 eV) to 6442 cm^{-1} (0.88 eV) are blueshifted from toluene (604 nm) over THF (589 nm) to dichloromethane (587 nm) and a decrease of the Stokes shifts from 10100 to 9800 cm^{-1} can be determined. The hypsochromic emission shift with increasing solvent polarity indicates a stabilization of the excited state in apolar solvents. Dual emission in dichloromethane might be caused by a twisted intramolecular charge transfer (TICT) state.[19] Upon photonic excitation the LE state equilibrates rapidly with the TICT state at lower energy.[20] This results in two emission maxima, one at higher energy (587 nm, emission from the LE state) and one at lower energy (760 nm, emission from the TICT state). The CIE coordinates clearly indicate orange emission colors (Figure S22). The intensity of the emission is low in THF and dichloromethane, in toluene it is stronger, but not that intense (Figure S22). Furthermore, the luminescence lifetimes fall

into the typical range for organic chromophores,[18] and range from 5.5 ns (toluene) to 12.0 ns (THF).

Figure S22. Emission of **BPN** in toluene, THF and dichloromethane (from left to right) (c = 10^{-4} mol/L, λ_{exc}= 365 nm).

Luminescence decay times (Solution state)

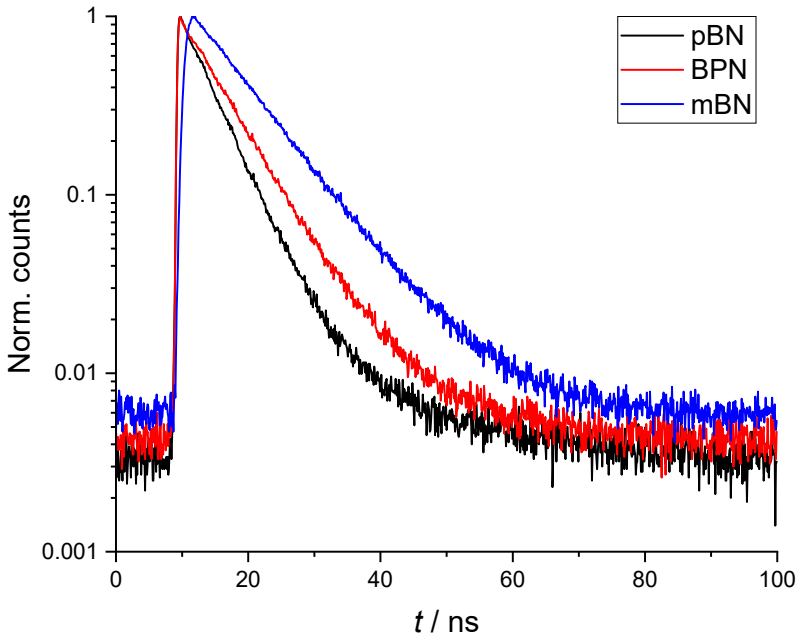

Figure S23. Photoluminescence decays for **pBN**, **mBN** and **BPN** recorded in toluene (c = 10^{-4} mol/L, T = 293 K).

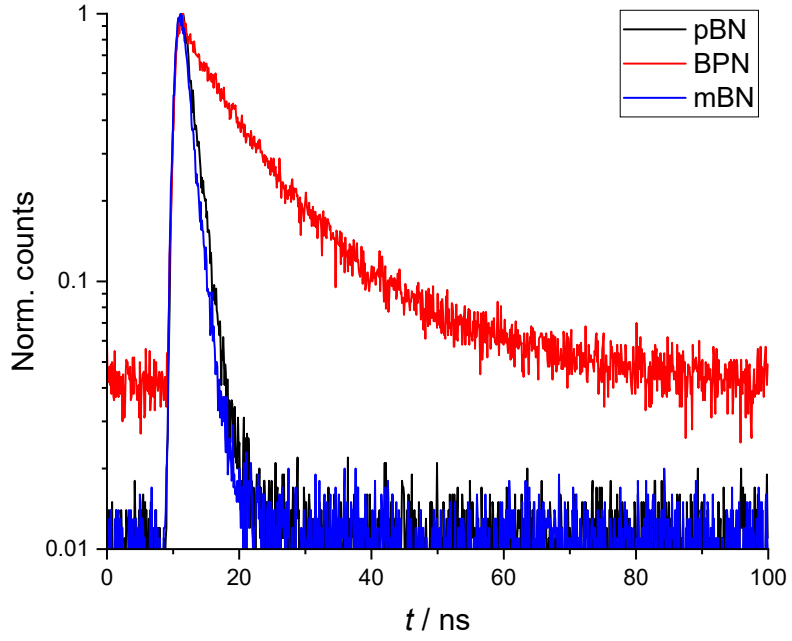

Figure S24. Photoluminescence decays for **pBN, mBN and BPN** recorded in THF (c = 10^{-4} mol/L, T = 293 K).

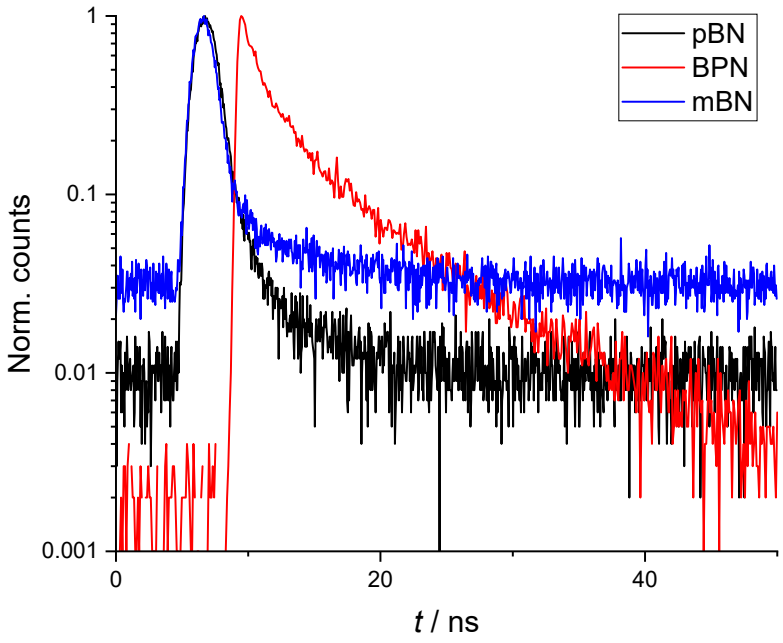

Figure S25. Photoluminescence decays for **pBN, mBN and BPN** recorded in dichloromethane (c = 10^{-4} mol/L, T = 293 K).

S6 Data of quantum chemical calculations

Table S4. Computed absorption and emission data for **BPN**, **mBN** and **pBN** in vacuum. Oscillator strengths *f* are only given when > 0, adiabatic energies are given in bold italics.

Molec.	Geom.	State	Spectral line / nm	Energy / eV	Composition
BPN	**S_0**	S_0	-	0.00	92% GS
		S_1	415	2.98	81% H-L
		S_2	412	2.00	81% H-(L+1)
		S_3	362	2.42	42% H-(L+2),30% H-(L+4),17% H-
		S_4	343 ***f = 0.10***	3.61	42% H-(L+3),35% H-(L+5)
		T_1	-	2.92	64% H-(L+2),26% H-(L+7),20% H-
		T_2	-	2.95	53% H-L, 12% H-(L+8)
	S_1	S_0	-	0.00	91% GS
		S_1	544	2.28 ***2.49***	84% H-L
		T_1	-	2.34	84% H-L
	T_1	S_0	-	0.00	91% GS
		S_1	-	2.28	84% H-L
		T_1	-	2.24 ***2.44***	84% H-L
pBN	**S_0**	S_0	-	0.00	94% GS
		S_1	401	3.09	88% H-L
		S_2	398	3.11	87% H-(L+1)
		S_3	351	3.53	71% H-(L+2),18% H-(L+4)
		S_4	338 ***f = 0.09***	3.67	77% H-(L+3)
		T_1	-	3.01	41% H-(L+2),38% H-(L+4)
		T_2	-	3.06	80% H-L
	S_1	S_0	-	0.00	93% GS
		S_1	-	2.57 ***2.70***	89% H-L
		T_1	-	2.54	89% H-L
	T_1	S_0	-	0.00	93% GS
		S_1	-	2.58	89% H-L
		T_1	-	2.54 ***2.67***	89% H-L
mBN	**S_0**	S_0	-	0.00	94% GS
		S_1	402 *f = 0.01*	3.08	78% H-L
		S_2	398 *f = 0.01*	3.11	78% H-(L+1)
		S_3	351 *f = 0.01*	3.54	73% H-(L+2)
		S_4	344 *f = 0.01*	3.60	73% H-(L+3), 11% H-(L+2)
		S_5	310	4.00	80% H-(L+4)
		S_6	296 ***f = 0.14***	4.20	82% H-(L+5)
		T_1	-	2.89	37% H-(L+1), 26% H-(L+4), 20%
		T_2	-	3.01	59% H-L, 24% H-(L+1)
	S_1	S_0	-	0.00	93% GS
		S_1	497	2.49 ***2.68***	89% H-L
		T_1		2.41	81% H-L
	T_1	S_0		0.00	93% GS
		S_1		2.51	89% H-L
		T_1		2.41 ***2.59***	79% H-L

	S_0	S_1
BPN	8.78°	0.01°
mBN	10.95°	1.49°
pBN	11.43°	0.01°

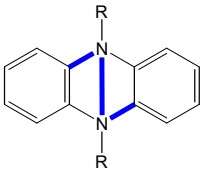

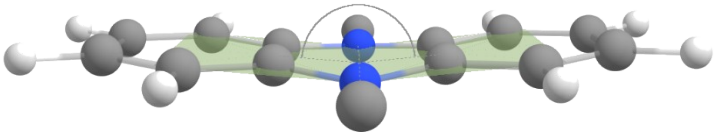

Figure S26. Phenazine-core planarization. Table entries denote the C-N-N-C dihedral angle in S_0 and S_1 geometries computed at the (TD)-DFT PBE0 level of theory.

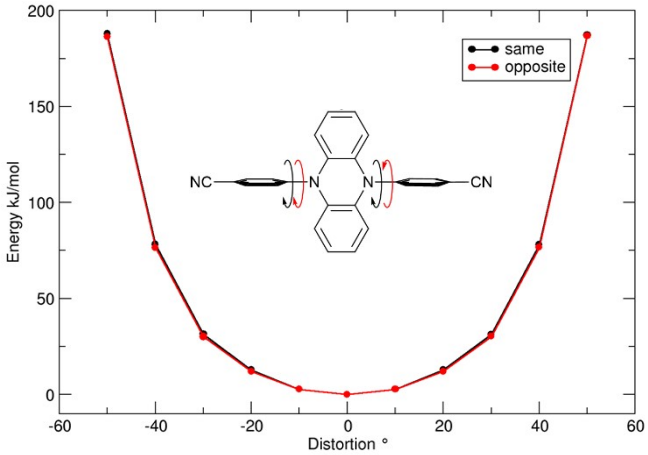

Figure S27. Unrelaxed dihedral scan for phenyl-rotation in **pBN** showing the energy profile (same and opposite directions phenyl rotation, the starting point corresponds to the perpendicular arrangement (90°) of phenazine and phenyl rings).

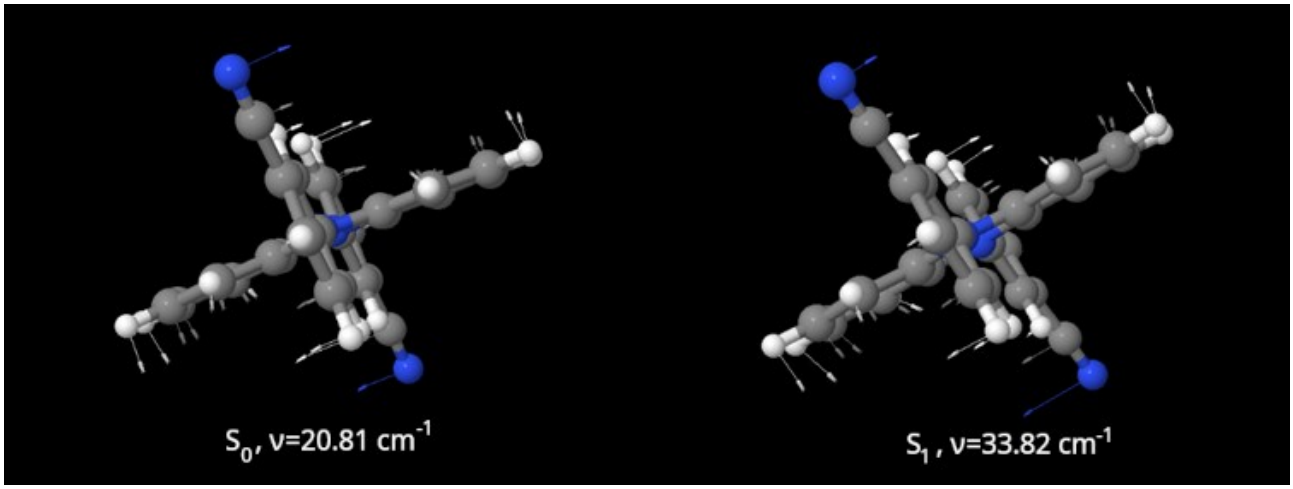

Figure S28. Normal mode vibrations including phenyl torsions in **mBN** (same direction) in S_0 (left) and S_1 (right) geometries.

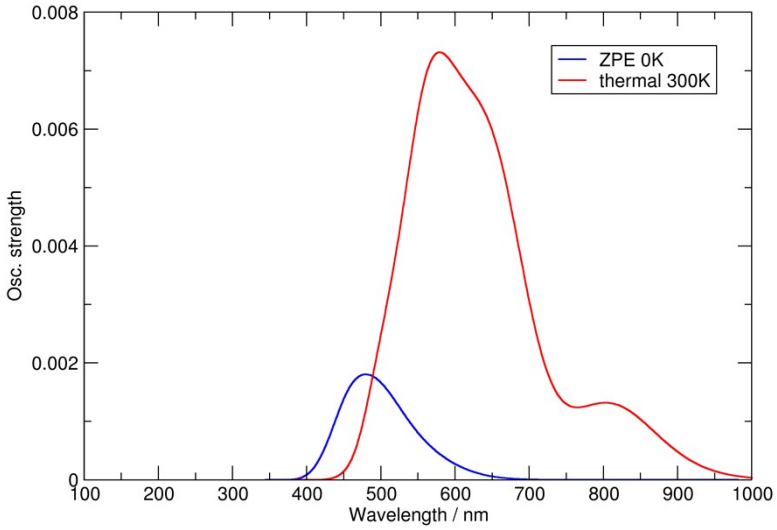

Figure S29. Computed emission in **pBN** at 0 K and 300 K (vacuum).

pBN s1	-45°	-30°	-15°	89.97°	+15°	+30°	+45°
-45°	0.280	0.281	0.176	0.081	0.039	0.087	0.286
-30°	0.287	0.175	0.188	0.083	0.041	0.081	0.174
-15°	0.284	0.172	0.075	0.034	0.076	0.173	0.286
89.97°	0.172	0.080	0.041	0.084	0.175	0.092	0.284
+15°	0.085	0.039	0.039	0.083	0.177	0.280	0.284
+30°	0.090	0.038	0.084	0.180	0.285	0.280	0.180
+45°	0.181	0.279	0.286	0.179	0.084	0.287	0.187

mBN s1	-45°	-30°	-15°	90.42°	+15°	+30°	+45°
-45°	0.174	0.175	0.128	0.103	0.101	0.106	0.177
-30°	0.175	0.128	0.138	0.108	0.104	0.105	0.126
-15°	0.175	0.128	0.105	0.106	0.107	0.128	0.176
89.63°	0.126	0.107	0.103	0.109	0.127	0.111	0.176
+15°	0.104	0.106	0.098	0.104	0.127	0.174	0.175
+30°	0.109	0.105	0.107	0.131	0.172	0.176	0.127
+45°	0.128	0.176	0.172	0.130	0.109	0.177	0.133

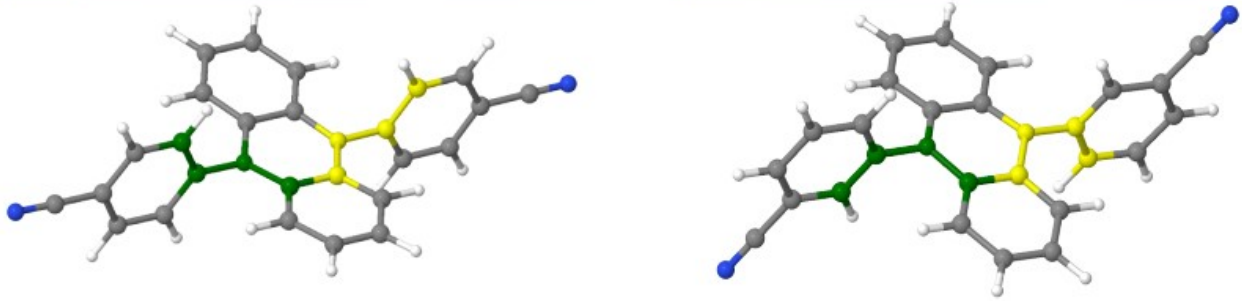

Figure S30. Modulation of ΔE_{ST} in **mBN** and **pBN**.

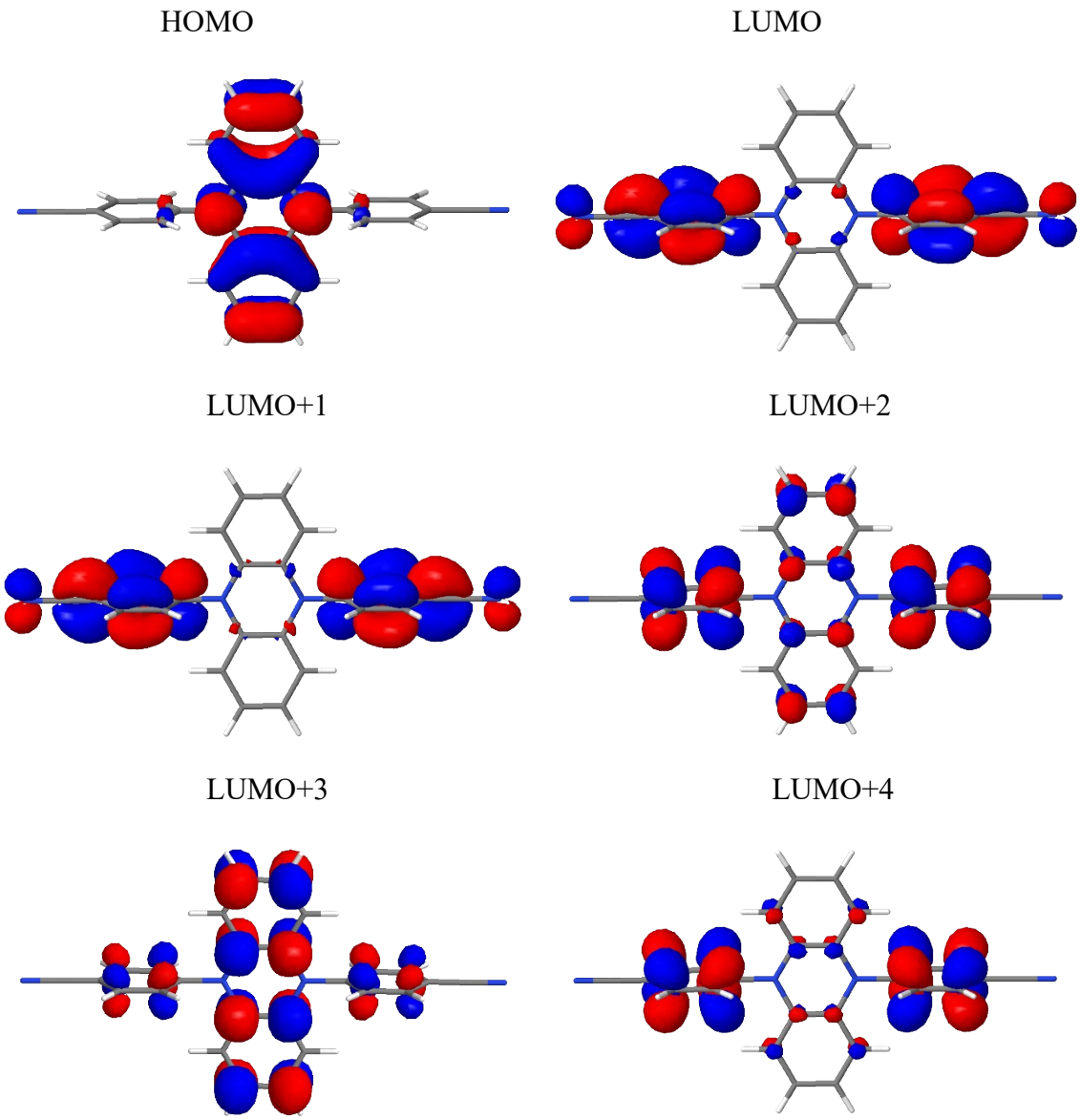

Figure S31. BH-LYP-computed orbitals involved in **pBN** excitations.

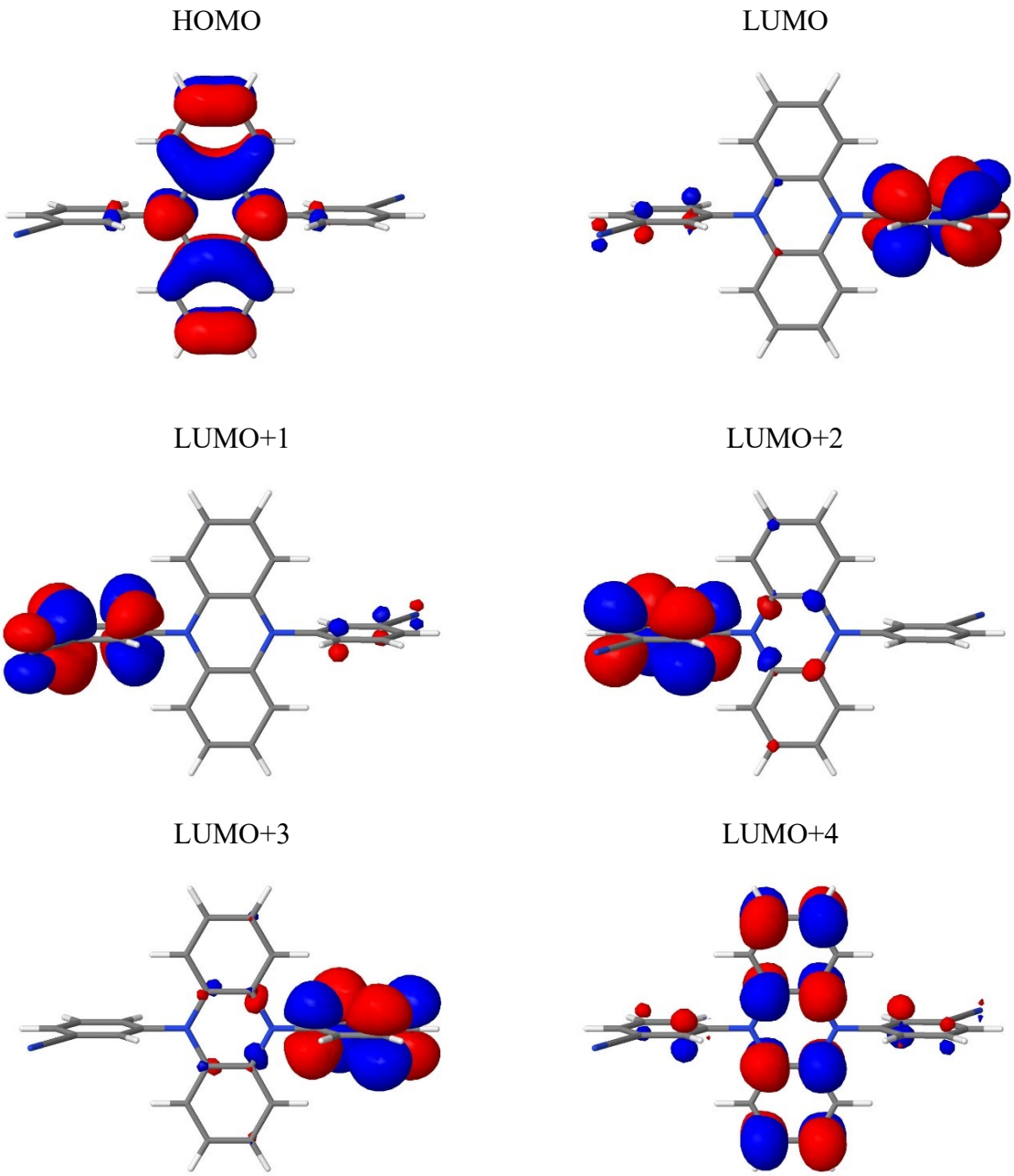

Figure S32. BH-LYP-computed orbitals involved in **mBN** excitations.

References

1. Lee, J.; Shizu, K.; Tanaka, H.; Nakanotani, H.; Yasuda, T.; Kaji, H.; Adachi, C. Controlled emission colors and singlet–triplet energy gaps of dihydrophenazine-based thermally activated delayed fluorescence emitters. *J. Mater. Chem. C.* **2015**, *3*, 2175-2181. https://doi.org/10.1039/c4tc02530j
2. Theriot, J.C.; Lim, C.-H.; Yang, H.; Ryan, M.D.; Musgrave, C.B.; Miyake, G.M. Organocatalyzed atom transfer radical polymerization driven by visible light. *Science* **2016**, *352*, 1082-1086. https://doi.org/10.1126/science.aaf3935
3. WO 2014/18922 A1
4. *APEX2, data collection program for the CCD area-detector system, Version 2.1-0*, *Bruker Analytical X-ray Systems*, Madison (WI), USA, 1997-2014.
5. *SAINT, data reduction and frame integration program for the CCD area-detector system*, *Bruker Analytical X-ray Systems*, Madison (WI), USA, 1997-2014.
6. CrysAlis^{Pro}, Rigaku Oxford Diffraction/Agilent Technologies UK Ltd, Yarnton, Great Britain, release 1.171.40.103a, **2021**.
7. Sheldrick, G.M. Crystal structure refinement with SHELXL. *Acta. Crystallogr. Sect. C Cryst. Struct. Commun.* **2015**, *C71*, 3–8. https://doi.org/10.1107/S2053229614024218.
8. Dolomanov, O.V.; Bourhis, L.J.; Gildea, R.J.; Howard, J.A.K.; Puschmann, H. OLEX2: A complete structure solution, refinement and analysis program. *J. Appl. Crystallogr*. **2009**, *42*, 339–341. https://doi.org/10.1107/S0021889808042726.
9. Brandenburg, K. Diamond 4.6, Crystal and Molecular Structure Visualization. Copyright 1997-2022 Crystal Impact GbR, Bonn, Germany. Available online: https://www.crystalimpact.com/diamond/ (accessed on 10 August 2022).
10. Q. Wan, Y. Li, K. Ding, Y. Xie, J. Fan, J. Tong, Z. Zeng, Y. Li, C. Zhao, Z. Wang, B. Z. Tang. Aggregation Effect on Multiperformance Improvement in Aryl-Armed Phenazine-Based Emitters. *J. Am. Chem. Soc.* **2023**, *145*, 1607−1616. https://doi.org/10.1021/jacs.2c09210
11. Spek, A.L. Structure validation in chemical crystallography. *Acta Crystallogr. D Biol. Crystallogr.* **2009**, *65*, 148–155, doi:10.1107/S090744490804362X.
12. Spek, A.L. *PLATON—A Multipurpose Crystallographic Tool*; Utrecht University: Utrecht, The Netherlands, 2008.
13. Farrugia, L.J. *Platon – Windows Implementation*; Version 270519; University of Glasgow: Scotland, UK, 2019.
14. Janiak, C. A critical account on π–π stacking in metal complexes with aromatic nitrogen-containing ligands. *J. Chem. Soc. Dalton Trans.* **2000**, 3885–3896. https://doi.org/10.1039/b003010o.
15. Yang, X.-J.; Drepper, F.; Wu, B.; Sun, W.-H.; Haehnel, W.; Janiak, C. From model compounds to protein binding: Syntheses, characterizations and fluorescence studies of $[Ru^{II}(bipy)(terpy)L]^{2+}$ complexes (bipy = 2,2'-bipyridine; terpy = 2,2':6',2''-terpyridine; L = imidazole, pyrazole and derivatives, cytochrome *c*). *Dalton Trans.*, **2005**, 256-267. http://dx.doi.org/10.1039/b414999h.
16. Nishio, M. The CH/π hydrogen bond in chemistry. Conformation, supramolecules, optical resolution and interactions involving carbohydrates. *Phys. Chem. Chem. Phys.* **2011**, *13*, 13873-13900. https://doi.org/10.1039/C1CP20404A.
17. Kamlet, M.J.; Abboud, J.L.; Taft, R.W. The Solvatochromic Comparison Method. 6. The π* Scale of Solvent Polarities. *J. Am. Chem. Soc.* **1977**, *99*, 6027-6038. https://doi.org/10.1021/ja00460a031
18. Lakowicz, J.R. (Ed.) *Principles of Fluorescence Spectroscopy;* Springer US, Boston, MA, **2006**.
19. Grabowski, Z.R.; Dobkowski, J. Twisted intramolecular charge transfer (TICT) excited states: energy and molecular structure. *Pure Appl. Chem.* **1983**, *55*, 245-252. https://doi.org/10.1351/pac198855020245
20. Sasaki, S.; Drummen, G.P.C.; Konishi, G. Recent advances in twisted intramolecular charge transfer (TICT) fluorescence and related phenomena in materials chemistry. *J. Mater. Chem. C* **2016**, *4*, 2731-2743. https://doi.org/10.1039/C5TC03933A